



Homogenization of interlocking masonry structures using a generalized differential expansion technique

I. Stefanou^a, J. Sulem^b and I. Vardoulakis[†]

^a *Department of Applied Mathematics and Physics
National Technical University of Athens
Zografou Campus, Greece
e-mail: istefanou@mechan.ntua.gr,
web page: <http://geolab.mechan.ntua.gr/>
(Corresponding author¹)*

^b *UR Navier, CERMES,
Ecole des Ponts ParisTec, Université Paris-Est,
Marne-la-Vallée, France
e-mail: sulem@cermes.enpc.fr
web page: <http://navier.enpc.fr/~sulem/index.html>*

Keywords: *Micromorphic Continuum; Interlocking masonry; Wave propagation; Generalized Differential Expansion; Homogenization.*

Abstract: In this paper a micromorphic continuum is derived for the homogenization of masonry structures with interlocking blocks. This is done by constructing a continuum which maps exactly the kinematics of the corresponding discrete masonry structure and has the same internal and kinetic energy for any ‘virtual’ translational- and rotational-field. The obtained continuum is an anisotropic micromorphic continuum of second order. The enriched kinematics of micromorphic continua allows to model microelement systems undergoing both translations and rotations. The homogenization technique applied here excludes averaging and keeps all the necessary information of the discrete structure. Therefore, all the dispersion curves of the discrete system are reproduced in the continuum model.

[†] Deceased

¹ Corresponding Author:

Ioannis Stefanou

Office address: Department of Applied Mathematics and Physics, National Technical University of Athens, P.O.BOX GR15780, Athens, Greece

Permanent address: 5-7, Chalkidos St., Chalandri, P.O.BOX GR15231, Athens, Greece

e-mail: istefanou@mechan.ntua.gr,

web page: <http://geolab.mechan.ntua.gr/>

tel: +30 697 7 212 890

fax: +30 210 67 22 873

1. Introduction

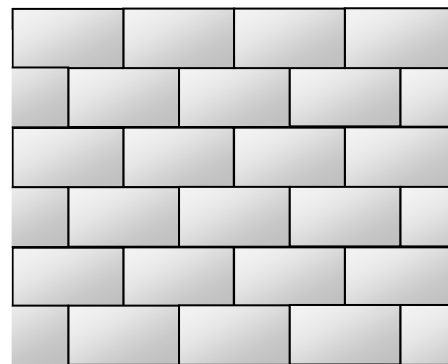
Masonry wall structures are usually formed by regularly distributed bricks and mortar following a certain periodic building pattern, i.e. the brickwork. Typical example of brickwork is the ‘running-bond’ pattern presented in figure 1. Generally, when the masonry walls consist of blocks of the same height they are called ‘isodomi’². In ancient times, the construction of such masonry was very expensive, considering the time and the technical difficulty for hewing hard stone blocks. Consequently, the construction of ‘isodomus’ brickwork is generally met only in luxurious buildings and temples, like Parthenon. However, from the structural point of view, the construction of masonry walls with building blocks of the same size, results to brickwork with limited or no interlocking. To face this, large tie-stones and special metal elements were used to bond the masonry building blocks together and to assure their interlocking. Observing ancient masonry structures, one could claim that the interlocking of the building blocks was an essential characteristic and a desired feature. Take for instance the masonry wall depicted in figure 2 **Erreur ! Source du renvoi introuvable.** from the civilization of Incas, the interlocking of the building blocks is apparent.

Following the ‘Homogenization by Differential Expansions Technique’ (Pasternak and Mühlhaus, 2005) the deformation and the dynamic behavior of the running-bond masonry wall patterns was investigated in the frame of continuum theory (cf. Masiani et al., 1995; Sulem and Mühlhaus, 1997; Cerrolaza et al., 1999; Stefanou et al., 2008 among others). The Cosserat continuum (Cosserat, 1909; Vardoulakis and Sulem, 1995) provided the necessary background to develop an equivalent continuum that maps the kinematics and the energy of these discrete masonry structures. Here, a different pattern is investigated (Figure 3). The geometrical difference between this pattern and the running-bond pattern is that it is constituted by two different in size and height interacting blocks. The running-bond and stack-bond patterns are degenerated cases of the aforementioned diatomic pattern and can be obtained by appropriately adjusting the dimensions of the building blocks of the present diatomic pattern (Figure 6). However, the structural difference and the practical importance of the diatomic pattern presented herein is the interlocking of the building blocks. Examining the diatomic texture of figure 3, we notice that no horizontal or vertical joints cut the masonry wall from side to side. This characteristic essentially contributes to the overall strength of the masonry structure under various loading situations.

The homogenization procedure followed herein differs from the above mentioned for the monatomic running-bond configurations. The main reason is that the Cosserat continuum is not sufficient to capture the six independent degrees of freedom of the diatomic masonry pattern (Stefanou et al., 2008). As it is will be shown later in the paper, the appropriate

² Latin, from the Greek word “ισόδομος” (*ίσο* + *δόμος* = equal + horizontal layer of building blocks) meaning built with blocks of equal height.

continuum that describes the dynamics of the structure is an anisotropic micromorphic continuum of second order. Generally, the enriched kinematics of micromorphic continua allows to model microelement systems undergoing both translations and rotations. The basic paper of Germain (1973) provides the theoretical background of higher order micromorphic continua. The present paper focuses on the use of higher order continuum theories for the homogenization of structural examples and emphasizes in the practical significance of the concepts and quantities that are introduced in generalized micromorphic continua. This is done by constructing a continuum which, for any ‘virtual’ translational- and rotational-field, maps exactly the kinematics of the corresponding lattice structure and has the same internal and kinetic energy. The domain of validity of the resulting micromorphic continuum is evaluated by comparing its dynamic response with the dynamic response of the lattice model. The dynamic response of a structure is characterized by its dispersion functions that relate the wave propagation frequency to the wavelength. Thus the dispersion functions of the homogenized continuum are compared with those of the discrete structure of blocks in order to assess the validity of the homogenization. Notice that if the homogenization procedure is inadequate, then the dispersion curves between the continuum and the discrete diverge, reflecting that the two systems have (a) different degrees of freedom, (b) different rigidities and (c) different inertial properties.

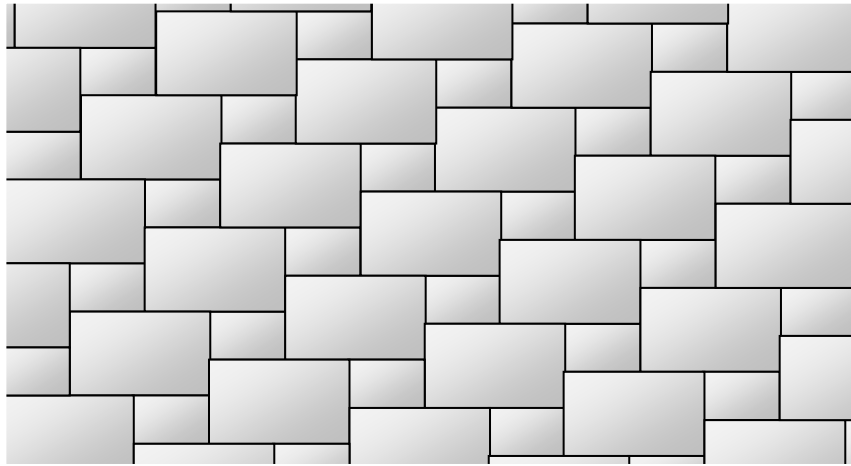


Running-bond

Figure 1. Running-bond masonry building pattern.



Figure 2. Interlocking blocks at masonry wall in Peru (I.Vardoulakis 2006).



Interlocking wall

Figure 3. Interlocking masonry pattern studied herein.

2. The discrete model

The masonry wall is constituted by two types of blocks (Figure 4). The first one (No.1), which will be called ‘small block’, has dimensions $a_1 \times b_1 \times d$, while the second (No.2), i.e. the ‘large block’, has dimensions $a_2 \times b_2 \times d$, where d is the thickness of the wall. Without any loss of generality, we assume: $a_2 \geq a_1$ and $b_2 \geq b_1$. The masses of the blocks are respectively m_1 and m_2 . The arrangement of the building blocks is periodic in space and it follows the pattern presented in figure 5. In solid state physics terminology (Kittel, 1996), this pattern is called ‘lattice’ while the repeated cell is called “basis”:

$$\text{structure} = \text{lattice} + \text{basis} \quad (1)$$

The basis or the “elementary cell”, as it is called here, must contain all the necessary information for the constitutive description of the periodic structure. It has to be mentioned though, that generally the elementary cell is not unique and that its choice affects the obtained homogenized continuum. For this rather well known point the reader can refer to the book of Novozhilov (1961).

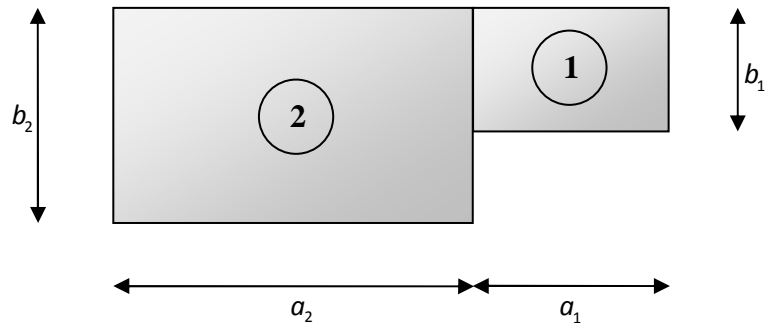


Figure 4. Elementary cell (basis) of the interlocking masonry wall and numbering of the blocks. Block No.1 has dimensions $a_1 \times b_1 \times d$ and mass m_1 while block No.2 has dimensions $a_2 \times b_2 \times d$ and mass m_2 . d is the thickness of the blocks.

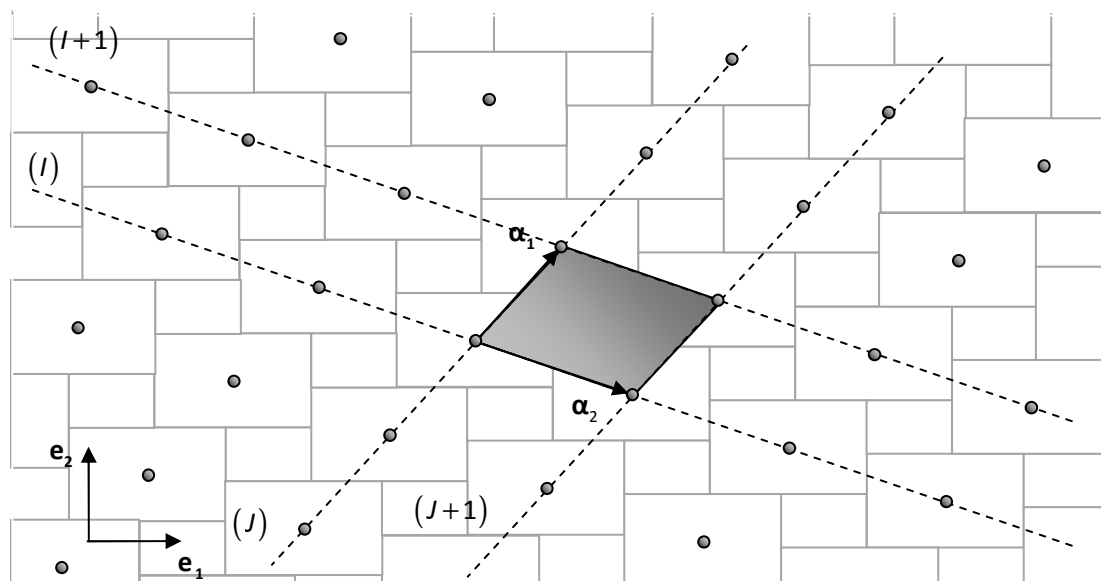


Figure 5. Periodic arrangement of the elementary cells and nodes of the lattice. The dark region denotes the chosen primitive cell of the lattice defined by the primitive axes α_i .

The chosen elementary cell of the lattice (basis), depicted in figure 4, is associated with the primitive cell defined by the primitive axes α_i (Figure 5). Note that a primitive cell is a minimum volume cell that fills all space by suitable repetition and translation. The interlocking masonry wall structure is generated by repeating and translating the chosen basis

over the lattice points. Translation is the simplest among 17 possible ways for generating a two dimensional pattern (Ernst, 1983). The lattice translational vector is (Kittel, 1996):

$$\mathbf{T}(n_1, n_2) = n_1 \boldsymbol{\alpha}_1 + n_2 \boldsymbol{\alpha}_2 \quad (2)$$

where n_i ($i=1,2$) are arbitrary integers and:

$$\begin{aligned} \boldsymbol{\alpha}_1 &= a_1 \mathbf{e}_1 + b_2 \mathbf{e}_2 \\ \boldsymbol{\alpha}_2 &= a_2 \mathbf{e}_1 - b_1 \mathbf{e}_2 \end{aligned} \quad (3)$$

\mathbf{e}_i are the unit vectors of the Cartesian global system.

Each node of the lattice is given two indices representing its position in space. Thus the coordinates of node (I, J) are:

$$\begin{aligned} X_1^{(I,J)} &= (I \boldsymbol{\alpha}_1 + J \boldsymbol{\alpha}_2) \mathbf{e}_1 \\ X_2^{(I,J)} &= (I \boldsymbol{\alpha}_1 + J \boldsymbol{\alpha}_2) \mathbf{e}_2 \end{aligned} \quad (4)$$

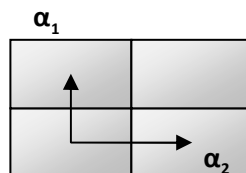
The nodes of the lattice coincide with the centers of mass of the large blocks. The centers of mass of the small blocks are:

$$\begin{aligned} X_1^{(I+\frac{1}{2}, J+\frac{1}{2})} &= \left[\left(I + \frac{1}{2} \right) \boldsymbol{\alpha}_1 + \left(J + \frac{1}{2} \right) \boldsymbol{\alpha}_2 \right] \mathbf{e}_1 \\ X_2^{(I+\frac{1}{2}, J+\frac{1}{2})} &= \left[\left(I + \frac{1}{2} \right) \boldsymbol{\alpha}_1 + \left(J + \frac{1}{2} \right) \boldsymbol{\alpha}_2 \right] \mathbf{e}_2 \end{aligned} \quad (5)$$

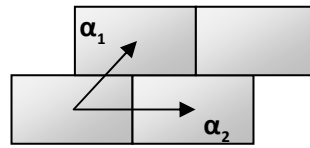
The volume of the elementary cell is:

$$V = \sum_{i=1}^2 a_i b_i d \quad (6)$$

Depending on the sizes of the blocks, various types of interlocking masonry wall structures can emerge. Figure 6 shows clearly that the running-bond and stack-bond patterns are degenerated cases of the general pattern.



$$\begin{aligned} a_1 &= 0 \\ b_1 &= 0 \end{aligned}$$



$$a_2 = 2a_1$$

$$b_1 = 0$$

Figure 6. Various patterns and configurations for different dimensions of the two building blocks. Notice that the running-bond and the stack-bond patterns are degenerated cases of the general interlocking pattern.

For the mechanical description of the structure we assume that the building blocks are rigid with deformable interfaces (soft-contacts). This assumption implies that the deformation is concentrated on the interfaces of the bricks and that it is small as compared to their dimensions. This assumption is verified especially in historical dry-masonry structures. Yet, even in the case of non dry-masonry structures, the rigidity of the interface (brick-mortar-brick) is smaller than the mortar itself (Raffard, 2000). Generally, the assumption of rigid building blocks with deformable interfaces is adopted by many researchers in similar approaches (cf. Besdo, 1985; Masiani et al., 1995; Sulem and Mühlhaus, 1997; Cecchi and Sab, 2004; Cecchi et al., 2007; Cecchi and Milani, 2008). A further assumption for the numerical examples that will follow is that the horizontal and vertical joints of the brickwork have the same mechanical properties. The developed stresses Σ^β at the interfaces of the blocks are assumed to be linearly distributed over them and the constitutive law of the joints is assumed to be linear elastic. The assumption of linear stress distribution is justified in (Milani et al., 2006), where the authors show that linear stress distributions at the interfaces give satisfying results as compared to constant and quadratic stress distributions. Consequently, the interfaces between the blocks transfer both forces and torques (Figure 7). Under the above assumptions the interaction of the blocks can be approximated by linear normal, tangential and rotational springs.

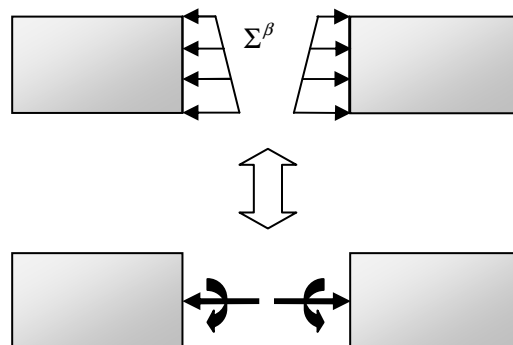


Figure 7. Normal stresses developed at interface Σ^β of the blocks and their equivalent forces and moments.

The aim of this paper is to discuss the appropriate continuum for interlocking structures. For simplicity it is here restricted to linear elastic interacting blocks. However it should be mentioned that masonry structures are generally characterized by strong non-linearities, and plastic behavior even at low levels of applied loading. The non-linear behavior of masonry is owed to the frictional behavior of the interfaces of the building blocks. Exceptions are some ancient masonry structures from the Classic and Hellenistic period, where the building blocks are tied together with special metal connectors (Bouras et al. 2002). The bonding of the building blocks through the aforementioned connectors extends the elastic domain of the deformations of the structure. As proposed for example by Sulem and Mühlhaus (1997), when an appropriate continuum is identified for representing a given structure, extension to non-linear behavior can be developed by considering the relevant failure mechanisms. A multi-mechanisms yield surface is then derived. Other examples based on limit analysis for the determination of the out-of-plane strength of masonry are proposed by Cecchi et al., (2007) and Cecchi and Milani (2008).

Wall deformations involve translations and rotations of the masonry blocks. For in-plane deformations the involved degrees of freedom (dof's) of each block are three. These are the translation parallel to \mathbf{e}_1 and \mathbf{e}_2 axes and the rotation around \mathbf{e}_3 axis. With $U_1^{(b)}$ and $U_2^{(b)}$ we denote the translation of the center mass of block b and with $\Omega_3^{(b)}$ the rotation. For infinitesimal rotations (small strains) the displacement of a point of a block b is:

$$P_i^{(b)}(R_j^{(b)}) = U_i^{(b)} - \varepsilon_{ij3} \Omega_3^{(b)} (R_j^{(b)} - C_j^{(b)}) \quad (7)$$

where ε_{ijk} is the Levi-Civita tensor, $C_i^{(b)}$ the center of mass of the block b and $R_i^{(b)}$ the position vector of the point of block b . With capital letters we refer to quantities expressed in the global coordinate system. In figure 8 the numbering of the interfaces of the elementary cell is shown. In particular the elementary cell interacts with the adjacent cells along ten interfaces $\Sigma^1 - \Sigma^{10}$ while the two blocks of the basis interact through the interface Σ^0 .

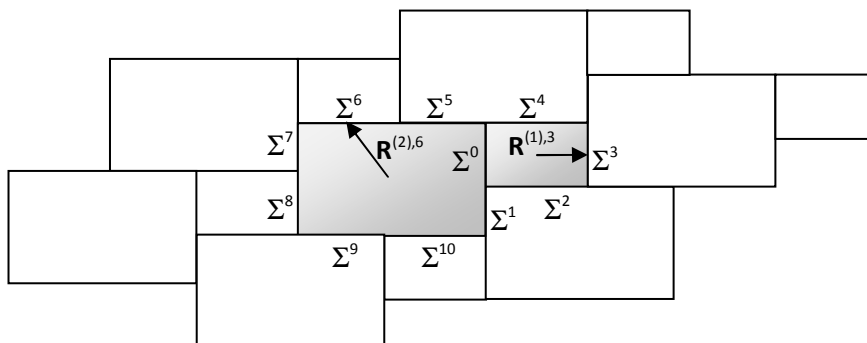


Figure 8. Numbering of interfaces Σ^β of the elementary cell with its adjacent cells and examples of the position vectors $R_j^{(b),\beta}$.

Let b^A, b^B be two blocks interacting through interface Σ^β and $F_i^{(b^A, b^B), \beta}$ (resp. $F_i^{(b^B, b^A), \beta}$) and $M_i^{(b^A, b^B), \beta}$ (resp. $M_i^{(b^B, b^A), \beta}$) the force and the moment exerted by block b^B over b^A (resp. b^A over b^B). Then a set of self-balanced forces and moments is developed in the lattice. This set is expressed as follows:

$$\begin{aligned} F_i^{(b^A, b^B), \beta} &= \mathbf{K}_{ij}^\beta \Delta U_j^{(b^A, b^B), \beta} \\ M_i^{(b^A, b^B), \beta} &= \Lambda^\beta \Delta \Omega_j^{(b^A, b^B), \beta} \end{aligned} \quad (8)$$

where $\Delta U_i^{(b^A, b^B), \beta} = P_i^{(b^A)}(R_j^{(b^A), \beta}) - P_i^{(b^B)}(R_j^{(b^B), \beta})$, $\Delta \Omega_j^{(b^A, b^B), \beta} = \Omega_3^{(b^A)} - \Omega_3^{(b^B)}$, $R_j^{(b), \beta}$ the position vector of the center of the area of interface Σ^β ,

$$\left(\mathbf{K}_{ij}^\beta \right) = \begin{cases} A_{V1} \begin{pmatrix} k_n & 0 \\ 0 & k_s \end{pmatrix}, \text{ for } \beta = 0, 3, 8 \\ A_{V2} \begin{pmatrix} k_n & 0 \\ 0 & k_s \end{pmatrix}, \text{ for } \beta = 1, 7 \\ A_{H1} \begin{pmatrix} k_s & 0 \\ 0 & k_n \end{pmatrix}, \text{ for } \beta = 4, 6, 10 \\ A_{H2} \begin{pmatrix} k_s & 0 \\ 0 & k_n \end{pmatrix}, \text{ for } \beta = 2, 5, 9 \end{cases}, \quad \Lambda^\beta = \begin{cases} A_{V1} \frac{b_1^2}{12} k_n, \text{ for } \beta = 0, 3, 8 \\ A_{V2} \frac{(b_2 - b_1)^2}{12} k_n, \text{ for } \beta = 1, 7 \\ A_{H1} \frac{a_1^2}{12} k_n, \text{ for } \beta = 4, 6, 10 \\ A_{H2} \frac{(a_2 - a_1)^2}{12} k_n, \text{ for } \beta = 2, 5, 9 \end{cases},$$

A_H (A_V) is the area of the horizontal (vertical) interface, k_n the normal- and k_s the shear-elastic stiffness of the interfaces with dimensions $\frac{[F]}{[L]^3}$ and specifically: $A_{H1} = a_1 d$, $A_{V1} = b_1 d$, $A_{H2} = (a_2 - a_1) d$, $A_{V2} = (b_2 - b_1) d$.

For rigid blocks, the elastic energy is only stored at the interfaces. The internal energy of the structure is:

$$\begin{aligned} \mathcal{U}_{usc} &= \frac{1}{2} \sum_{el} \left[\sum_{\beta=1}^{10} \left(\frac{1}{2} F_i^{(b^A, b^B), \beta} \Delta U_j^{(b^A, b^B), \beta} + \frac{1}{2} M_i^{(b^A, b^B), \beta} \Delta \Omega_j^{(b^A, b^B), \beta} \right) \right] \\ &+ \sum_{el} \left(\frac{1}{2} F_i^{(b^A, b^B), 0} \Delta U_j^{(b^A, b^B), 0} + \frac{1}{2} M_i^{(b^A, b^B), 0} \Delta \Omega_j^{(b^A, b^B), 0} \right) \end{aligned} \quad (9)$$

where V is the volume of the elementary cell (cf. Eq.(6)), and \sum_{el} indicates the sums over all the elementary cells of the structure.

The power density of internal forces of the elementary cell is given by:

$$p_{cell} = \frac{1}{V} \sum_{\beta=0}^5 \left(F_i^{(b^A, b^B), \beta} \Delta \dot{U}_j^{(b^A, b^B), \beta} + M_i^{(b^A, b^B), \beta} \Delta \dot{\Omega}_j^{(b^A, b^B), \beta} \right) \quad (10)$$

where $\dot{q} = \frac{dq}{dt}$.

The power of internal forces of the structure is thus:

$$\mathcal{P}_{dsc} = \sum_{el} V p_{cell} \quad (11)$$

Similarly, the kinetic energy of the structure is:

$$\mathcal{K}_{dsc} = \sum_{el} V k_{cell} \quad (12)$$

and the kinetic energy density of the elementary cell is:

$$k_{cell} = \frac{1}{V} \sum_{b=1}^2 \left(\frac{1}{2} m_b \dot{U}_i^{(b)} \dot{U}_i^{(b)} + \frac{1}{2} \mathbf{J}_b \dot{\Omega}_3^{(b)2} \right) \quad (13)$$

where $m_b = \rho a_b b_b d$ and $\mathbf{J}_b = \frac{1}{12} m_b (b_b^2 + a_b^2)$ and ρ the density of the blocks. The inertia tensor \mathbf{J}_b is expressed at principal axes.

The equations of motion for each individual block b of the masonry structure are:

$$\begin{aligned} \frac{\partial \mathcal{U}_{dsc}}{\partial U_1^{(b)}} &= m_b \ddot{U}_1^{(b)} \\ \frac{\partial \mathcal{U}_{dsc}}{\partial U_2^{(b)}} &= m_b \ddot{U}_2^{(b)} \\ \frac{\partial \mathcal{U}_{dsc}}{\partial \Omega_3^{(b)}} &= J_b \ddot{\Omega}_3^{(b)} \end{aligned} \quad (14)$$

We seek solutions to Eq.(14) of the form:

$$\begin{aligned} U_i^{(l,J)} &= \mathcal{U}_i^{(2)} e^{i[\kappa(l\alpha_1 + J\alpha_2) - \omega t]} \\ \Omega_3^{(l,J)} &= \mathcal{W}^{(2)} e^{i[\kappa(l\alpha_1 + J\alpha_2) - \omega t]} \\ U_i^{(l+\frac{1}{2}, J+\frac{1}{2})} &= \mathcal{U}_i^{(1)} e^{i\left[\kappa\left[\left(l+\frac{1}{2}\right)\alpha_1 + \left(J+\frac{1}{2}\right)\alpha_2\right] - \omega t\right]} \\ \Omega_3^{(l+\frac{1}{2}, J+\frac{1}{2})} &= \mathcal{W}^{(1)} e^{i\left[\kappa\left[\left(l+\frac{1}{2}\right)\alpha_1 + \left(J+\frac{1}{2}\right)\alpha_2\right] - \omega t\right]} \end{aligned} \quad (15)$$

where $i = \sqrt{-1}$, $\boldsymbol{\kappa} = \kappa(\cos\theta \mathbf{e}_1 + \sin\theta \mathbf{e}_2)$, κ the wave number and θ the direction of the propagating wave.

The wavelength and the group velocity of the propagating waves are respectively:

$$\lambda = \frac{2\pi}{\kappa} \quad (16)$$

$$c = \frac{\omega}{\kappa}$$

For convenience we introduce the following dimensionless quantities:

$$\hat{a}_b = \frac{a_b}{L}, \quad \hat{b}_b = \frac{b_b}{L}, \quad \hat{d} = \frac{d}{L}, \quad \hat{k}_n = \frac{k_n}{\rho g}, \quad \hat{k}_s = \frac{k_s}{\rho g}, \quad \hat{u}_{disc} = \frac{u_{disc}}{\rho g L^4},$$

$$\hat{m}_b = \frac{m_b}{\rho L^3}, \quad \hat{j}_b = \frac{j_b}{\rho L^4}, \quad \hat{U}_i = \frac{U_i}{L}, \quad d\tau = \sqrt{\frac{g}{L}} dt, \quad \hat{\kappa} = L\kappa, \quad \hat{\omega} = \sqrt{\frac{L}{g}} \omega, \quad (17)$$

$$\hat{\lambda} = \frac{\lambda}{L}, \quad \hat{c} = \sqrt{\frac{1}{gL}} c, \quad L = V^{1/3}$$

In the numerical examples that follow the dimensions of the blocks are $a_1 = 250mm$, $b_1 = 125mm$, $a_2 = 500mm$, $b_2 = 250mm$ and $d = 1000mm$. The specific weight of the bricks is $20kN/m^3$, the thickness of the joints $10mm$, the Young's Modulus of the mortar $4GPa$ and the Poisson's ratio 0.2 . Consequently, the dimensionless elastic normal and shear-stiffness of the interfaces are $\hat{k}_n = 2 \cdot 10^7$ and $\hat{k}_s = 0.8 \cdot 10^7$.

Because of the six degrees of freedom of the elementary cell, six dispersion functions of the structure are obtained and presented in figures 9 and 10. Each dispersion curve corresponds to a different oscillation mode, which activates different degrees of freedom of the blocks. For example for the above numerical parameters and for large wave lengths ($\hat{\kappa} \rightarrow 0$), oscillation modes 1 and 2 are characterized by the translation of both blocks (No.1&2), which dominates their rotation, while oscillation mode 3 is characterized by the rotation of the blocks (acoustic branches). For the higher frequency oscillation modes, 4 and 6, the translations of the blocks of the elementary cell are in 180° phase (opposite directions), while for oscillation mode 5 the rotations of the building blocks of the elementary cell are in 180° phase (optic branches).

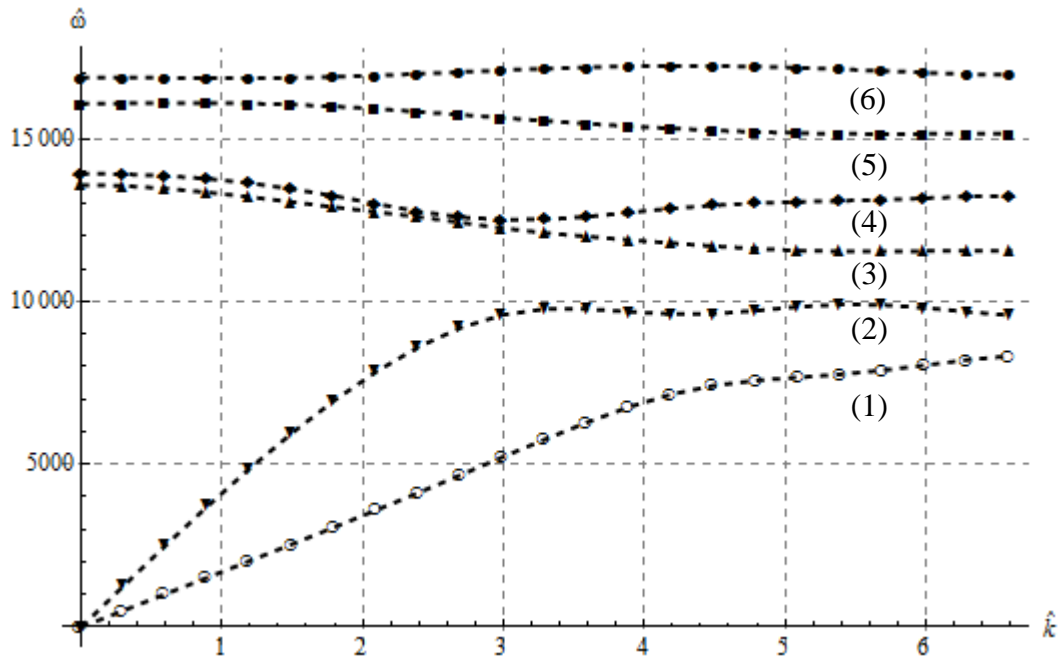


Figure 9. Dispersion functions ($\hat{\omega}(\hat{k})$) of propagating waves in direction e_1 . Six dispersion functions are derived because of the six degrees of freedom of the elementary cell. Each dispersion curve corresponds to a different oscillation mode (No. 1 to 6).

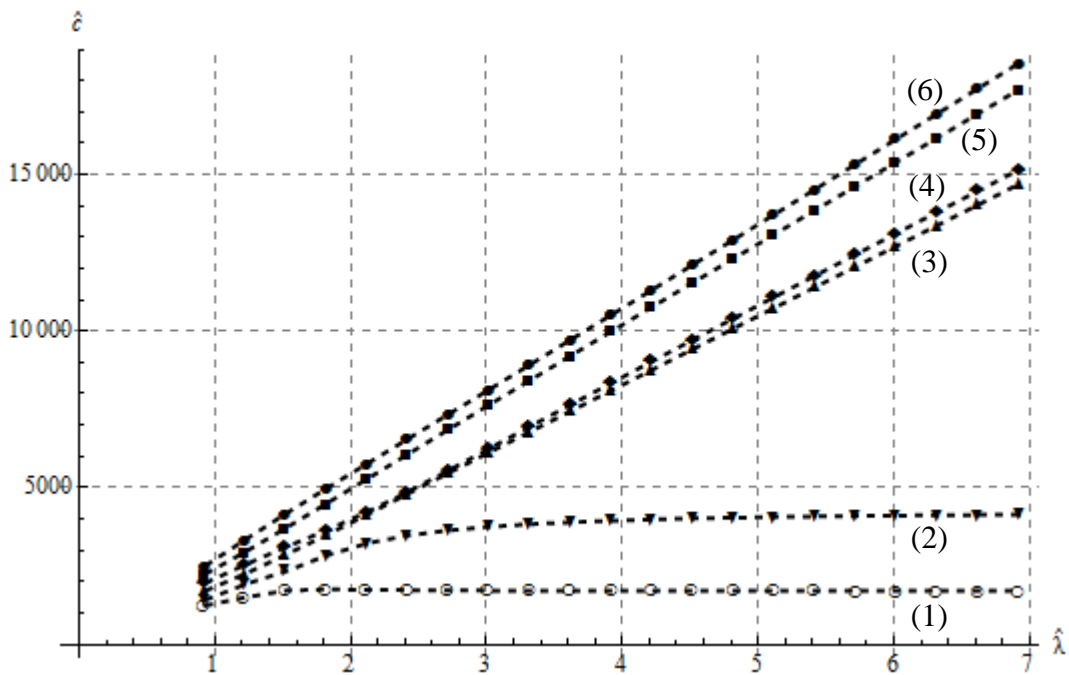


Figure 10. Dispersion functions ($\hat{c}(\hat{\lambda})$) of propagating waves in direction e_1 . Six dispersion functions are derived because of the six degrees of freedom of the elementary cell. Each dispersion curve corresponds to a different oscillation mode (No. 1 to 6).

3. The continuous model

The enriched kinematics of generalized micromorphic continua makes them suitable for describing materials with microstructure. As opposed to the static regime (Salerno and de Felice, 2009), in the dynamic regime the richer the structure of the continuum model is, the more refined the homogenization (identification) scheme should be. Otherwise, the dispersion functions of the continuous approximation would not converge to the discrete ones, which would contradict the equivalence between the continuum and the discrete system.

The homogenization procedure followed here is based on the construction of a continuum, which satisfies the two following criteria:

- The kinematics of the discrete system is identical to the kinematics of the continuum.
- The power of the internal forces and the kinetic energy of the continuum are equal to the power of the internal forces and the kinetic energy of the discrete system for any virtual kinematic field.

The main steps of the method proposed here are presented in figure 11.

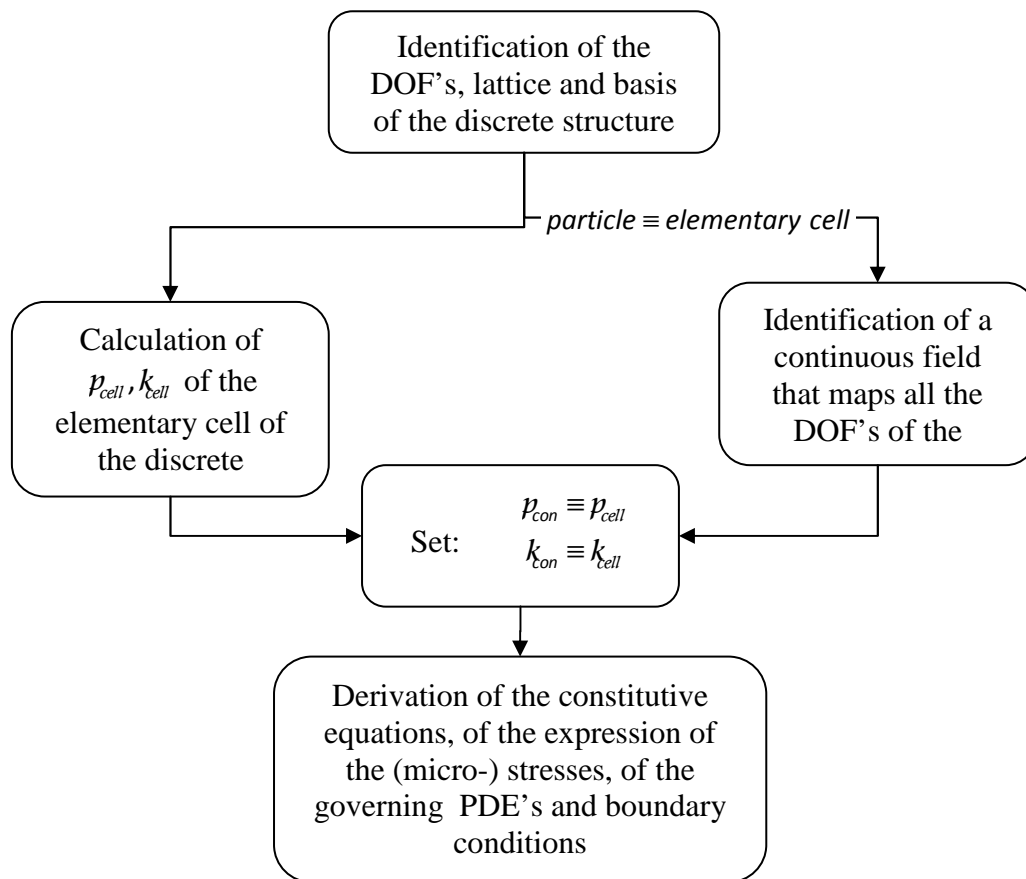


Figure 11. Main steps of the method for the derivation of a continuum describing the discrete structure. PDE means Partial Differential Equation and DOF Degree Of Freedom.

The formulation presented here follows Germain (1973), by identification of the elementary cell to the particle of the corresponding micromorphic continuum:

$$particle \equiv elementary \ cell \quad (18)$$

Therefore, in the specific case of the in-plane deformation of the interlocking masonry wall, the particle $P(M)$ should have six degrees of freedom (2 translational and 1 rotational for each block in 2D). Therefore, approaches through classical or micropolar continuum are inappropriate to capture the full dynamics of the discrete system. Assuming a system of particles and following Germain's notation (1973), M is the center of mass of the particle $P(M)$, M' a point of $P(M)$, V_i^c the velocity of M , x'_i the coordinates of M' in a Cartesian frame parallel to the given frame X_i with M its origin, V'_i the velocity of M' with respect to the given frame and X_i the coordinates of M in the given frame (Figure 12). D denotes the control volume. For a given particle, it is natural to look at the Taylor expansion of V'_i with respect to x'_j :

$$V'_i = V_i^c + \chi_{ij} x'_j + \chi_{ijk} x'_j x'_k + \chi_{ijkl} x'_j x'_k x'_l + \dots \quad (19)$$

χ_{ij} , χ_{ijk} and χ_{ijkl} are called micro-deformation rate tensors. Assuming that V'_i is continuous in x'_i , the tensors χ_{ijk} and χ_{ijkl} are fully symmetric with respect to the indices j, k, l .

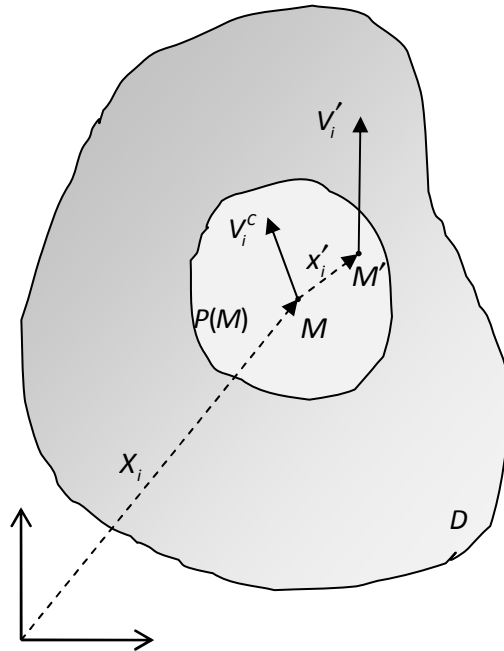


Figure 12. Continuum with microstructure.

The identification of the particle with the elementary cell (Eq.(18)) results in the following definitions that relate the velocities of the continuous with the velocities of the discrete model:

$$\begin{aligned}
\dot{U}_i^{(i,j)} &\triangleq V'_i(\mathbf{r}'^{(2)}) \\
\dot{\Omega}_3^{(i,j)} &\triangleq -\frac{1}{2} \left[V'_{1,2}(\mathbf{r}'^{(2)}) - V'_{2,1}(\mathbf{r}'^{(2)}) \right] \\
\dot{U}_i^{(i+\frac{1}{2},j+\frac{1}{2})} &\triangleq V'_i(\mathbf{r}'^{(1)}) \\
\dot{\Omega}_3^{(i+\frac{1}{2},j+\frac{1}{2})} &\triangleq -\frac{1}{2} \left[V'_{1,2}(\mathbf{r}'^{(1)}) - V'_{2,1}(\mathbf{r}'^{(1)}) \right]
\end{aligned} \tag{20}$$

where $(\cdot)_{,i} = \frac{\partial(\cdot)}{\partial x'_i}$ ($i=1,2$) and $\mathbf{r}'^{(b)}$ the coordinates of the center mass of block 'b' in a Cartesian frame parallel to the given frame X_i with M its origin:

$$\begin{aligned}
\mathbf{r}'^1 &= \mu_2 \mathbf{\Delta} \\
\mathbf{r}'^2 &= -\mu_1 \mathbf{\Delta}
\end{aligned} \tag{21}$$

where $\mathbf{\Delta} = \frac{1}{2} \begin{bmatrix} a_1 + a_2 \\ b_2 - b_1 \end{bmatrix}$ and $\mu_1 = \frac{m_1}{m_1 + m_2}$, $\mu_2 = \frac{m_2}{m_1 + m_2}$.

It should be mentioned that the rotations of the blocks in Eqs.(20) are defined in the continuum through the *Curl* of the vector field V'_i , $\nabla \times V'_i$. Additionally we define the following quantities:

$$\begin{aligned}
\dot{E}_{ij}^{(i,j)} &\triangleq \frac{1}{2} \left[V'_{i,j}(\mathbf{r}'^{(2)}) + V'_{j,i}(\mathbf{r}'^{(2)}) \right] \\
\dot{E}_{ij}^{(i+\frac{1}{2},j+\frac{1}{2})} &\triangleq \frac{1}{2} \left[V'_{i,j}(\mathbf{r}'^{(1)}) + V'_{j,i}(\mathbf{r}'^{(1)}) \right]
\end{aligned} \tag{22}$$

$\dot{E}_{ij}^{(b)}$ may be interpreted as a homogeneous deformation rate tensor of the blocks themselves in the elementary cell. Notice that this interpretation is not necessary for the particular case of the interlocking masonry wall considered here as we do not have additional dof's describing the individual deformation of the blocks. However, such an interpretation is more systematic and allows to generalize the approach and to consider also deformable blocks. For rigid blocks it holds:

$$\begin{aligned}
\frac{1}{2} \left[V'_{i,j}(\mathbf{r}'^{(2)}) + V'_{j,i}(\mathbf{r}'^{(2)}) \right] &= 0 \\
\frac{1}{2} \left[V'_{i,j}(\mathbf{r}'^{(1)}) + V'_{j,i}(\mathbf{r}'^{(1)}) \right] &= 0
\end{aligned} \tag{23}$$

Equations (20) and (22) map exactly the discrete dof's to the continuum dof's. Consequently, from the continuum point of view, the dislocations and the disclinations that appear at the interfaces of the blocks have no effect on the derived continuum. We focus here only on the centers of the blocks of the structure and, therefore, there is no implication of field discontinuities in the formulation of the equivalent continuum. Combining Eqs. (20) and (22) we obtain:

$$\begin{aligned}
 \dot{U}_1^{(i,j)} &= V_1^c - \frac{\Delta_1(\mu_1 + 3\mu_2)\chi_{11}\mu_1}{6\mu_2} - \Delta_2\chi_{12}\mu_1 - \Delta_2^2\chi_{212}\mu_1^2 \\
 \dot{U}_2^{(i,j)} &= V_2^c - \frac{\Delta_2\mu_1(\mu_1 + 3\mu_2)\chi_{22}}{6\mu_2} + \Delta_1\mu_1(\chi_{12} + \Delta_2\mu_1\chi_{212}) \\
 \dot{\Omega}_3^{(i,j)} &= -\chi_{12} - 2\Delta_2\mu_1\chi_{212} \\
 \dot{U}_1^{(i+\frac{1}{2},j+\frac{1}{2})} &= V_1^c + \frac{\Delta_1(3\mu_1 + \mu_2)\chi_{11}\mu_2}{6\mu_1} + \Delta_2\chi_{12}\mu_2 - \Delta_2^2\chi_{212}\mu_2^2 \\
 \dot{U}_2^{(i+\frac{1}{2},j+\frac{1}{2})} &= V_2^c + \frac{\Delta_2\mu_2(3\mu_1 + \mu_2)\chi_{22}}{6\mu_1} + \Delta_1\mu_2(\Delta_2\mu_2\chi_{212} - \chi_{12}) \\
 \dot{\Omega}_3^{(i+\frac{1}{2},j+\frac{1}{2})} &= -\chi_{12} + 2\Delta_2\mu_2\chi_{212}
 \end{aligned} \tag{24}$$

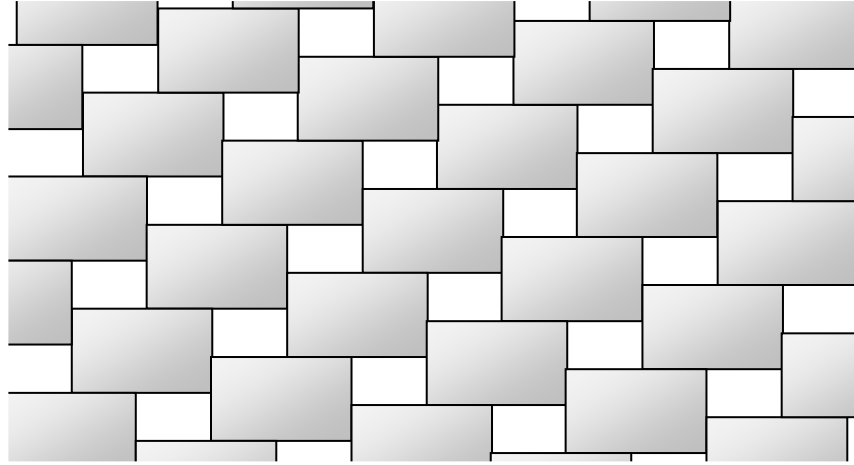
together with the following linear constraints for the other higher order kinematical quantities:

$$\begin{aligned}
 \chi_{1111} &= -\frac{\chi_{11}}{3\Delta_1^2\mu_1\mu_2} \\
 \chi_{2222} &= -\frac{\chi_{22}}{3\Delta_2^2\mu_1\mu_2} \\
 \chi_{111} &= \frac{(\mu_2 - \mu_1)\chi_{11}}{2\Delta_1\mu_1\mu_2} + \frac{\chi_{212}\Delta_2^2}{\Delta_1^2} \\
 \chi_{222} &= \frac{(\mu_2 - \mu_1)\chi_{22}}{2\Delta_2\mu_1\mu_2} - \frac{\Delta_1\chi_{212}}{\Delta_2} \\
 \chi_{112} &= -\frac{\Delta_2\chi_{212}}{\Delta_1} \\
 \chi_{21} &= -\chi_{12}
 \end{aligned} \tag{25}$$

where in the above equations $V_i^c = V_i^c(X_m^{(i,j)}) = V_i^{c(i,j)}$, $\chi_{ij} = \chi_{ij}(X_m^{(i,j)}) = \chi_{ij}^{(i,j)}$,

$\chi_{ijk} = \chi_{ijk}(X_m^{(i,j)}) = \chi_{ijk}^{(i,j)}$, $\chi_{ijk\ell} = \chi_{ijk\ell}(X_m^{(i,j)}) = \chi_{ijk\ell}^{(i,j)}$. The remaining terms of Eq.(19) are zero.

The presence of the 2nd order term χ_{212} in Eq.(24) implies that a 2nd order micromorphic continuum will be needed to describe the microstructure. Alternatively, 3rd order terms $\chi_{ijk\ell}$ of microdeformation measures could be kept as independent quantities. However, this would result in a 3rd order micromorphic continuum, which is not necessary in the present case of rigid building blocks. It is worth noticing, that if μ_1 or μ_2 vanish a Cosserat continuum would be sufficient to describe the microstructure. A Cosserat continuum or, in the general case, a micromorphic continuum would be derived independently of the presence of internal moments. The case in which μ_1 or μ_2 are null represents a discrete masonry structure with voids (Figure 13).



Masonry wall with voids

Figure 13. Masonry wall with voids, which can be described by a Cosserat continuum.

Equations (24) can be inverted to give:

$$\begin{aligned}
 v_1^c &= \dot{U}_1^{(i,j)} + \Delta_2 \mu_1 \mu_2 (\mu_1 - \mu_2) \dot{\Omega}_3^{(i,j)} + \mu_1^2 (1 + 2\mu_2) \Delta \dot{U}_1 + \Delta_2 \mu_1^2 \mu_2 \Delta \dot{\Omega}_3 \\
 v_2^c &= \dot{U}_2^{(i,j)} - \Delta_1 \mu_1 \mu_2 (\mu_1 - \mu_2) \dot{\Omega}_3^{(i,j)} + \mu_1^2 (1 + 2\mu_2) \Delta \dot{U}_2 - \Delta_1 \mu_1^2 \mu_2 \Delta \dot{\Omega}_3 \\
 \chi_{11} &= \frac{3\mu_1 \mu_2}{\Delta_1} \left[2\Delta \dot{U}_1 + \Delta_2 (\Delta \dot{\Omega}_3 + 2\dot{\Omega}_3^{(i,j)}) \right] \\
 \chi_{22} &= \frac{3\mu_1 \mu_2}{\Delta_2} \left[2\Delta \dot{U}_2 - \Delta_1 (\Delta \dot{\Omega}_3 + 2\dot{\Omega}_3^{(i,j)}) \right] \\
 \chi_{12} &= -\dot{\Omega}_3^{(i,j)} - \mu_1 \Delta \dot{\Omega}_3 \\
 \chi_{212} &= \frac{1}{2\Delta_2} \Delta \dot{\Omega}_3
 \end{aligned} \tag{26}$$

where $\Delta \dot{U}_i = \dot{U}_i^{(\frac{1}{2}, \frac{1}{2})} - \dot{U}_i^{(i,j)}$, $\Delta \dot{\Omega}_3 = \dot{\Omega}_3^{(\frac{1}{2}, \frac{1}{2})} - \dot{\Omega}_3^{(i,j)}$ and $\Delta_1 \neq 0$, $\Delta_2 \neq 0$.

If blocks No.1 and No.2 are fixed together (through interface Σ^0), i.e. if the elementary cell is behaving as a rigid block, then:

$$\begin{aligned}
 \Delta \dot{U}_1 &= -\Delta_2 \dot{\Omega}_3^{(i,j)} \\
 \Delta \dot{U}_2 &= \Delta_1 \dot{\Omega}_3^{(i,j)} \\
 \Delta \dot{\Omega}_3 &= 0
 \end{aligned} \tag{27}$$

In this case, introducing Eqs.(27) into Eqs.(26) we deduce that a Cosserat continuum would be again sufficient to describe the microstructure with the two blocks fixed. In particular, the following relationships would hold:

$$\begin{aligned}
V_1^c &= \mu_1 \dot{U}_1^{\left(I+\frac{1}{2}, J+\frac{1}{2}\right)} + \mu_2 \dot{U}_1^{(I, J)} \\
V_2^c &= \mu_1 \dot{U}_2^{\left(I+\frac{1}{2}, J+\frac{1}{2}\right)} + \mu_2 \dot{U}_2^{(I, J)} \\
\chi_{12} &= -\dot{\Omega}_3^{\left(I+\frac{1}{2}, J+\frac{1}{2}\right)} = -\dot{\Omega}_3^{(I, J)} \\
\chi_{11} &= \chi_{22} = \chi_{212} = 0
\end{aligned} \tag{28}$$

Equations (20)-(26) refer to the kinematics of the elementary cell itself. At this point we need to pass from the microdeformation of the elementary cell to the macrodeformation of the assembly of the elementary cells. As the interaction of the elementary cell is limited to their first neighbors, a first order Taylor expansion from particle to particle of the velocities and microdeformation rate tensors is sufficient:

$$\begin{aligned}
V_i^{C(I+n_1, J+n_2)} &= V_i^{C(I, J)} + T_j (n_1, n_2) \dot{U}_{i, j}^{C(I, J)} \\
\chi_{ij}^{(I+n_1, J+n_2)} &= \chi_{ij}^{(I, J)} + T_k (n_1, n_2) \kappa_{ijk}^{(I, J)} \\
\chi_{ijk}^{(I+n_1, J+n_2)} &= \chi_{ijk}^{(I, J)} + T_\ell (n_1, n_2) \kappa_{ijk\ell}^{(I, J)}
\end{aligned} \tag{29}$$

where $(\cdot)_{,i} = \frac{\partial(\cdot)}{\partial \chi_i}$ ($i = 1, 2$), $\kappa_{ijk} = \chi_{ij,k}$, and $\kappa_{ijk\ell} = \chi_{ijk,\ell}$.

A first order Taylor expansion of the kinematic fields (from particle to particle) seems suitable for most applications. Exceptions are the applications where the forces between the elementary cells (particles) are not limited to the first neighbor (Mindlin, 1965). In other words, when the elementary cell does not interact only with its adjacent elementary cell but further with the second, third, etc. neighbor cells, higher order derivatives of the velocities and micro-deformation rates are needed. Alternatively, the elementary cell (particle) could be enlarged to contain all the interacting neighbors, but the price for this would be a higher order micromorphic continuum.

The power of internal forces for a Micromorphic continuum of 2nd order is given as follows (Germain, 1973):

$$p_{con} = \tau_{ij} V_{i,j}^c - (s_{ij} \chi_{ij} + s_{ijk} \chi_{ijk}) + (v_{ijk} \kappa_{ijk} + v_{ijk\ell} \kappa_{ijk\ell}) \tag{30}$$

with

$$\tau_{ij} \triangleq \sigma_{ij} + s_{ij} \tag{31}$$

where τ_{ij} is the stress tensor, σ_{ij} is the intrinsic stress tensor (symmetric), s_{ij} is the intrinsic microstress tensor, v_{ijk} is the intrinsic second microstress tensor and s_{ijk} , $v_{ijk\ell}$ are higher order stress tensors.

Having defined and linked the kinematics of the discrete and of the continuum, we set for any virtual kinematic field V_i^c , χ_{ij} , χ_{ijk} , $\chi_{ijk\ell}$, the power of the internal forces of the discrete system to be equal to the power of the internal forces of the continuum:

$$p_{con} \equiv p_{cell} \quad (32)$$

The same equality is set for the kinetic energy densities:

$$k_{con} \equiv k_{cell} \quad (33)$$

By introducing Eqs. (24) into Eq.(10) and using Eqs.(30) and (32) we derive the constitutive equations of the continuous:

$$\begin{aligned} \tau_{ij} &= \frac{\partial p_{con}}{\partial V_{i,j}^c} \\ s_{ij} &= -\frac{\partial p_{con}}{\partial \chi_{ij}}, \quad s_{ijk} = -\frac{\partial p_{con}}{\partial \chi_{ijk}} \\ v_{ijk} &= \frac{\partial p_{con}}{\partial \kappa_{ijk}}, \quad v_{ijk\ell} = \frac{\partial p_{con}}{\partial \kappa_{ijk\ell}} \end{aligned} \quad (34)$$

The tensors derived by Eqs.(34) are expressed as functions of the internal forces and moments of the elementary cell. For example:

$$\begin{aligned} \tau_{11} &= \frac{a_2}{V} \left(-F_1^{(b^A, b^B),1} + F_1^{(b^A, b^B),2} + F_1^{(b^A, b^B),3} \right) + \frac{a_1}{V} \left(F_1^{(b^A, b^B),3} + F_1^{(b^A, b^B),4} - F_1^{(b^A, b^B),5} \right) \\ s_{11} &= \frac{\Delta_1}{6V\mu_1\mu_2} \left(F_1^{(b^A, b^B),0} + F_1^{(b^A, b^B),2} + F_1^{(b^A, b^B),3} + F_1^{(b^A, b^B),4} \right) \end{aligned} \quad (35)$$

where b^A and b^B are blocks that belong to the elementary cell (I, J) , and its neighbors, and interact through interface β .

Through this formulation yield criteria can be set out in the continuum at the macrolevel by considering the internal forces and moments developed at the microlevel, i.e. at the interfaces of the microstructure. Various yielding mechanisms such as sliding, rocking and twisting can be considered and expressed in terms of internal forces and moments at the microlevel (e.g. Sulem and Mühlhaus, 1997). Failure criteria at the microlevel depend on the mechanical properties of the building blocks and their interfaces. These mechanical properties of the interfaces can be either specified according to existing interface models (Orduña and Lourenço, 2005; Milani et al. 2006) or determined experimentally on a per case basis. Thus, the plastic and, more generally, the non-linear macroscopic behavior of masonry can be considered and modeled accordingly by deriving the homogenized failure surfaces. Of course, this is not something new and has been successfully attempted in the past using the Differential Expansion homogenization technique for the in-plane deformation of the running-bond masonry pattern (Sulem and Mühlhaus, 1997). With the present

homogenization procedure the formulation of macroscopic failure criteria based on micromechanical considerations is straightforward, given the complexity of the derived continuum. Nevertheless, the development of failure criteria and yield surfaces is beyond the scope of the present paper, which focuses mainly on the construction of higher order continua to describe geometrically complex discrete systems.

Notice that as the wall spans only in directions \mathbf{e}_1 and \mathbf{e}_2 and only the in-plane degrees of freedom of the building blocks were taken into account, the derived continuum is two dimensional. Following a variational approach, the dynamic partial differential equations of the aforementioned 2nd order two dimensional micromorphic continuum developed here are:

$$\begin{aligned}
 \tau_{11,1} + \tau_{12,2} + f_1 &= \rho \Gamma_1 \\
 \tau_{21,1} + \tau_{22,2} + f_2 &= \rho \Gamma_2 \\
 \nu_{111,1} + \nu_{112,2} + s_{11} &= \rho \Gamma_{11} \\
 \nu_{121,1} + \nu_{122,2} + s_{12} &= \rho \Gamma_{12} \\
 \nu_{221,1} + \nu_{222,2} + s_{22} &= \rho \Gamma_{22} \\
 \nu_{2121,1} + \nu_{2122,2} + s_{212} &= \rho \Gamma_{212}
 \end{aligned} \tag{36}$$

where ρ is the mass density of the continuum (ρ is approximated by the mass density of the bricks of the wall structure, which is considered constant), f_i are long range volumic forces, i.e. the self-weight of the bricks, and:

$$\begin{aligned}
\Gamma_1 &= \gamma_1 + \frac{1}{6}\Delta_1(\mu_2 - \mu_1)\gamma_{11} - \Delta_2^2\mu_1\mu_2\gamma_{212} \\
\Gamma_2 &= \gamma_2 + \frac{1}{6}\Delta_2(\mu_2 - \mu_1)\gamma_{22} + \frac{1}{6}\Delta_1\Delta_2\mu_1\mu_2\gamma_{212} \\
\Gamma_{11} &= \frac{1}{6}\Delta_1(\mu_2 - \mu_1)\gamma_1 + \frac{\Delta_1^2(\mu_1^4 + 5\mu_2\mu_1^3 + 4\mu_2^2\mu_1^2 + 5\mu_2^3\mu_1 + \mu_2^4)}{36\mu_1\mu_2}\gamma_{11} \\
&\quad + \frac{1}{6}\Delta_1\Delta_2\gamma_{12} + \frac{1}{6}\Delta_1\Delta_2^2(\mu_1 - \mu_2)(\mu_1^2 + 3\mu_2\mu_1 + \mu_2^2)\gamma_{212} \\
\Gamma_{12} &= \frac{1}{6}\Delta_1\Delta_2\gamma_{11} + \left[\mu_1\mu_2(\Delta_1^2 + \Delta_2^2) + \frac{J_1 + J_2}{\rho V} \right] \gamma_{12} - \frac{1}{6}\Delta_1\Delta_2\gamma_{22} \\
&\quad + \Delta_2 \left[2\mu_1 \frac{J_2}{\rho V} + 2\mu_2 \frac{J_1}{\rho V} + \mu_1\mu_2(\mu_1 - \mu_2)(\Delta_1^2 + \Delta_2^2) \right] \gamma_{212} \\
\Gamma_{22} &= \frac{1}{6}\Delta_2(\mu_2 - \mu_1)\gamma_2 + \frac{\Delta_2^2(\mu_1^4 + 5\mu_2\mu_1^3 + 4\mu_2^2\mu_1^2 + 5\mu_2^3\mu_1 + \mu_2^4)}{36\mu_1\mu_2}\gamma_{22} \\
&\quad - \frac{1}{6}\Delta_1\Delta_2\gamma_{12} - \frac{1}{6}\Delta_1\Delta_2^2(\mu_1 - \mu_2)(\mu_1^2 + 3\mu_2\mu_1 + \mu_2^2)\gamma_{212} \\
\Gamma_{212} &= -\mu_1\mu_2\Delta_2^2\gamma_1 + \mu_1\mu_2\Delta_1\Delta_2\gamma_2 + \frac{1}{6}\Delta_1(\mu_1 - \mu_2)(\mu_1^2 + 3\mu_2\mu_1 + \mu_2^2)\Delta_2^2\gamma_{11} \\
&\quad + \Delta_2 \left[2\mu_1 \frac{J_2}{\rho V} - 2\mu_2 \frac{J_1}{\rho V} + \mu_2(\Delta_1^2 + \Delta_2^2)\mu_1(\mu_1 - \mu_2) \right] \gamma_{12} \\
&\quad - \frac{1}{6}\Delta_1(\mu_1 - \mu_2)(\mu_1^2 + 3\mu_2\mu_1 + \mu_2^2)\Delta_2^2\gamma_{22} \\
&\quad + \Delta_2^2 \left(\mu_2\mu_1(\Delta_1^2 + \Delta_2^2)(\mu_1^3 + \mu_2^3) + 4\mu_1^2 \frac{J_2}{\rho V} + 4\mu_2^2 \frac{J_1}{\rho V} \right) \gamma_{212}
\end{aligned} \tag{37}$$

$$\begin{aligned}
\gamma_i &= \frac{\partial V_i^c}{\partial t} \\
\gamma_{ij} &= \frac{\partial \chi_{ij}}{\partial t} \\
\gamma_{ijk} &= \frac{\partial \chi_{ijk}}{\partial t}
\end{aligned} \tag{38}$$

Assuming small deformations, the normal time derivative in Eqs.(38) is identical to the material derivative. Therefore, non-linearities are avoided. The inertia terms are derived by using Eqs.(33) and (13). Notice, that the microinertia terms in Eqs.(37) consist only in time derivatives and do not contain spatial derivatives as in the case of restricted continua (Georgiadis and Velgaki, 2003). The boundary conditions are given by Eqs.(26), for the part of the boundary where the displacements and rotations of the bricks of the elementary cells are prescribed and by the following equation for the complementary part of the boundary where generalized tractions are imposed:

$$\begin{aligned}
\mathbf{T}_i &= \tau_{ij}n_j \\
\mathbf{M}_{ij} &= v_{ijk}n_k \\
\mathbf{M}_{212} &= v_{212\ell}n_\ell
\end{aligned} \tag{39}$$

where n_i is the unit vector of the boundary.

The aforementioned generalized tractions are related to the forces and moments applied to the blocks of the microstructure as follows:

$$\begin{aligned}
T_i &= F_i^{ex,1} + F_i^{ex,2} \\
M_{ij} &= \frac{\Delta_i}{6\mu_1\mu_2} \left[F_i^{ex,1} (2\mu_1 + 1)\mu_2^2 - F_i^{ex,2} (1 + 2\mu_2)\mu_1^2 \right] \\
M_{12} &= -M^{ex,1} - M^{ex,2} + F_2^{ex,2}\Delta_1\mu_1 - F_1^{ex,2}\Delta_2\mu_1 - F_2^{ex,1}\Delta_1\mu_2 + F_1^{ex,1}\Delta_2\mu_2 \\
M_{212} &= \Delta_2 \left[2\mu_2 M^{ex,1} - 2\mu_1 M^{ex,2} + \mu_1^2 (F_2^{ex,2}\Delta_1 - F_1^{ex,2}\Delta_2) + \mu_2^2 (F_2^{ex,1}\Delta_1 - F_1^{ex,1}\Delta_2) \right]
\end{aligned} \tag{40}$$

where $F_i^{ex,b}$ and $M^{ex,b}$ are respectively the resultant force and moment of the forces exerted at the boundary of the block 'b', transferred to the center of mass of the block. Obviously, a free boundary has zero generalized traction. Notice that for a discrete masonry with voids (μ_1 or μ_2 is zero) $M_{ij} = M_{212} = 0$ and only Cosserat boundary conditions have to be specified. For instance, if the small blocks are replaced by voids ($\mu_1 = 0$) then the boundary conditions that have to be specified are:

$$\begin{aligned}
T_i &= F_i^{ex,2} \\
M_{12} &= -M^{ex,2} \\
M_{ij} &= M_{212} = 0
\end{aligned} \tag{41}$$

4. Application for the case of a structure with linear elastic interfaces

For linear elastic interfaces, as in the discrete description (Eqs.(8)), the constitutive law (Eqs.(34)) can be directly determined in function of the deformation measures of the continuum. The structure of the derived constitutive law equations is:

$$S = C X \tag{41}$$

where $S = \{\tau_{ij}, s_{11}, s_{22}, s_{12}, s_{212}, v_{11i}, v_{22i}, v_{12i}, v_{212i}\}$, $X = \{V_{ij}^C, \chi_{11}, \chi_{22}, \chi_{12}, \chi_{212}, \kappa_{11i}, \kappa_{22i}, \kappa_{12i}, \kappa_{212i}\}$, C a matrix containing the constitutive relations and $i = 1, 2$. The full form of Eqs.(41) is too long to be presented here. All the analytical calculations in the present paper have been performed with the symbolic language mathematical package Mathematica. The Mathematica files are available to the reader upon request.

To evaluate the dispersion functions, we seek solutions of Eqs.(36) of the form:

$$\begin{aligned}
V_i^C &= -\omega i \gamma_i^C e^{i(\kappa \cos \theta x_1 + \kappa \sin \theta x_2 - \omega t)} \\
\chi_{ij} &= -\omega i \chi_{ij} e^{i(\kappa \cos \theta x_1 + \kappa \sin \theta x_2 - \omega t)} \\
\chi_{ijk} &= -\omega i \chi_{ijk} e^{i(\kappa \cos \theta x_1 + \kappa \sin \theta x_2 - \omega t)}
\end{aligned} \tag{42}$$

Using the same parameters with Section 2 we calculate the six dispersion curves of the derived equivalent continuum (Figure 14, Figure 15). Each dispersion curve corresponds to a different oscillation mode, which activates different degrees of freedom of the blocks. Similar to the discrete model, for large wave lengths ($\hat{\kappa} \rightarrow 0$), the oscillation modes 1 and 2 are characterized by the translation of the blocks, while oscillation mode 3 is characterized by their rotations (acoustic branches). For the higher frequency oscillation modes 4, 5 and 6 the oscillations of the blocks of the elementary cell are in 180° phase (optic branches).

Figure 16 and figure 18 show that the discrete and the continuum descriptions converge asymptotically as the wavelength increases. Actually, the relative error, as defined below and for the parameters considered in the present numerical example, is less than 5% for $\hat{\lambda} \geq 10$ or 10% for $\hat{\lambda} \geq 5$.

$$\bar{e}_\%(\hat{c}) = \sum_{m=1}^6 \left| \frac{\hat{c}_{con}(m) - \hat{c}_{dsc}(m)}{\hat{c}_{con}(m)} \right| \quad (43)$$

Therefore, the continuum derived in the previous sections is a large wavelength approximation of the discrete system (Figure 17). This is acceptable in most civil engineering applications. The domain of validity of the continuous model may be enlarged to cover smaller wavelengths. This can be accomplished by choosing a larger elementary cell that contains more building blocks. However, this choice of larger elementary cells would result into a higher order micromorphic continuum which makes the continuum model more complex.

The effect of the direction of the propagating waves on the relative error between the continuum and discrete descriptions is shown in figure 19. The fact that the error is not uniform for all directions of the propagating wave is related to the anisotropy of the structure.

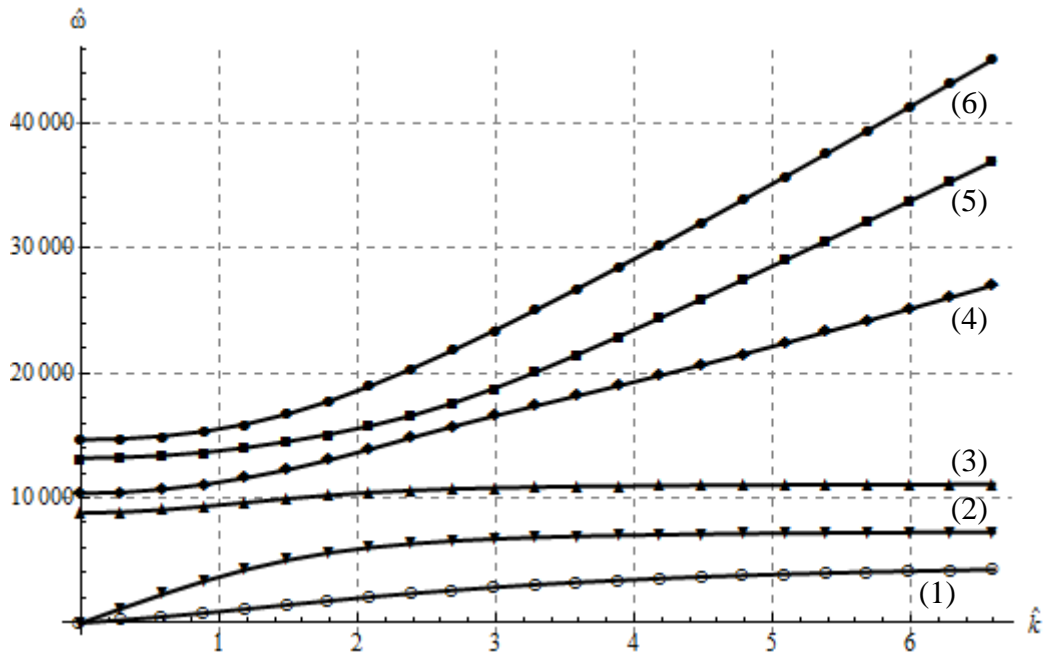


Figure 14. Dispersion functions ($\hat{\omega}(\hat{k})$) of propagating waves in direction e_1 . Six dispersion functions are derived because of the six independent deformation measures of the equivalent continuum. Each dispersion curve corresponds to a different oscillation mode (No. 1 to 6).

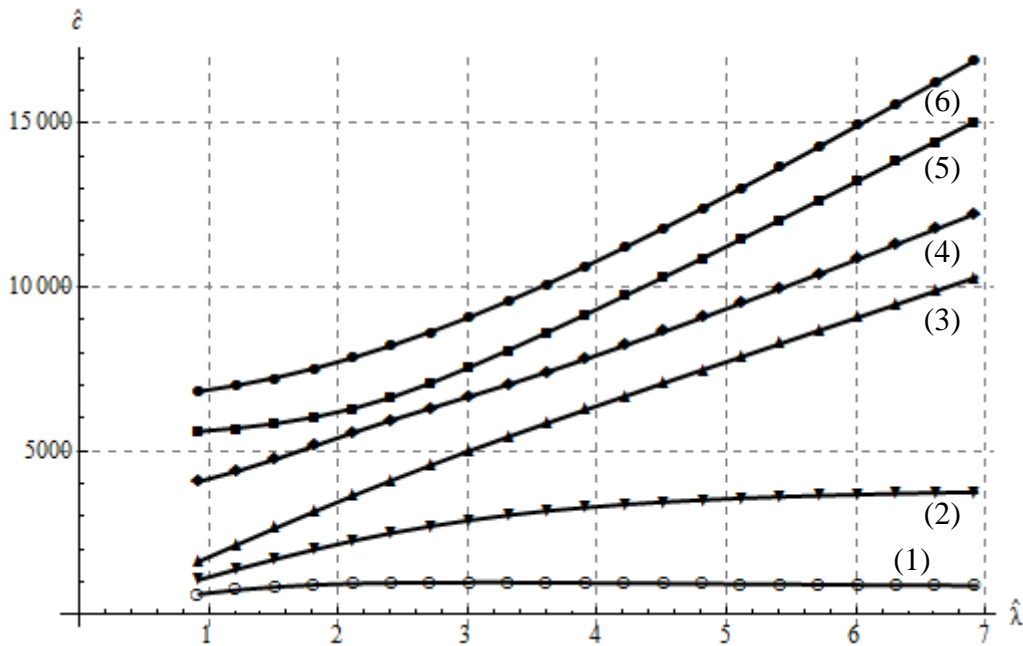


Figure 15. Dispersion functions ($\hat{c}(\hat{\lambda})$) of propagating waves in direction e_1 . Six dispersion functions are derived because of the six independent deformation measures of the equivalent continuum. Each dispersion curve corresponds to a different oscillation mode (No. 1 to 6).

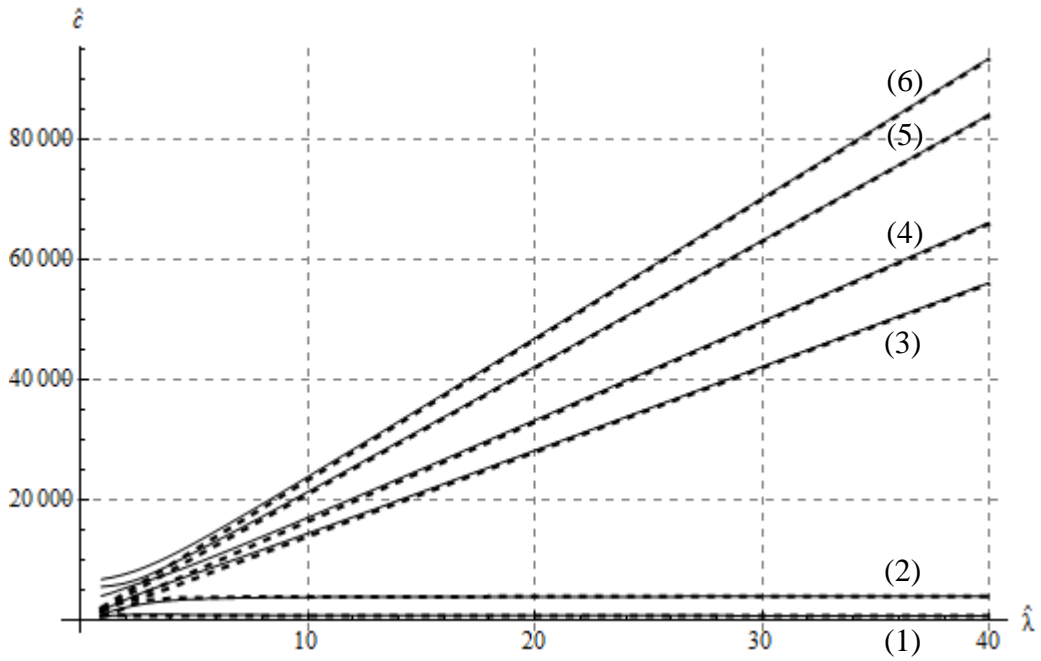


Figure 16. Comparison of the discrete (dashed lines) and continuum (solid lines) dispersion functions for propagating waves in direction e_1 . Continuum and discrete dispersion functions are identical for large wavelengths.

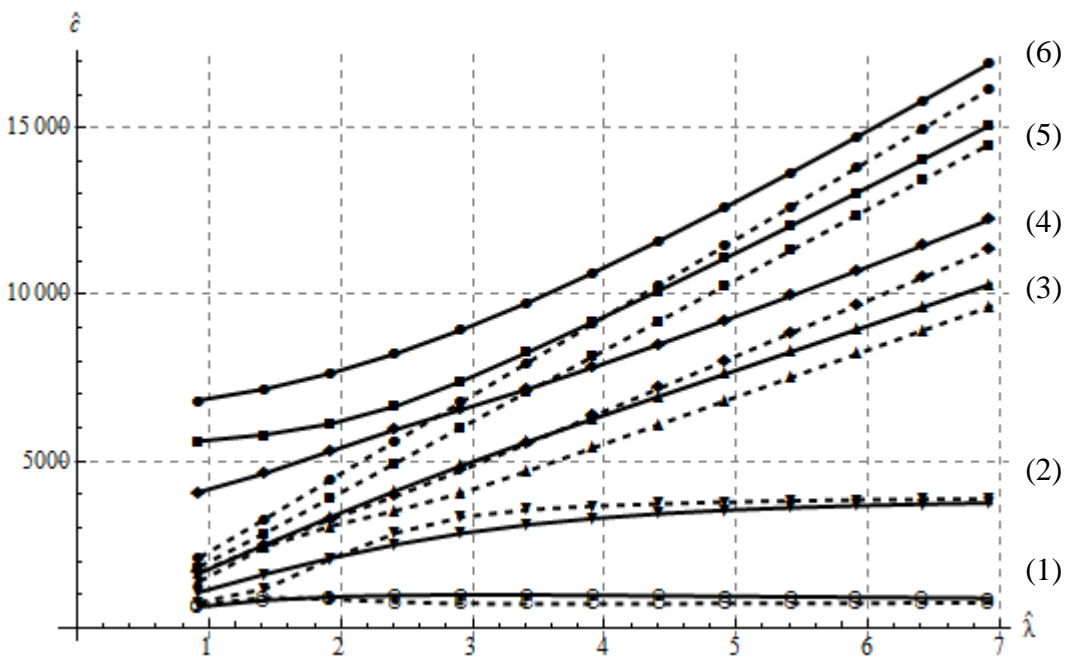


Figure 17. Divergence for small wavelengths of the discrete (dashed lines) and continuum (solid lines) dispersion functions for propagating waves in direction e_1 .

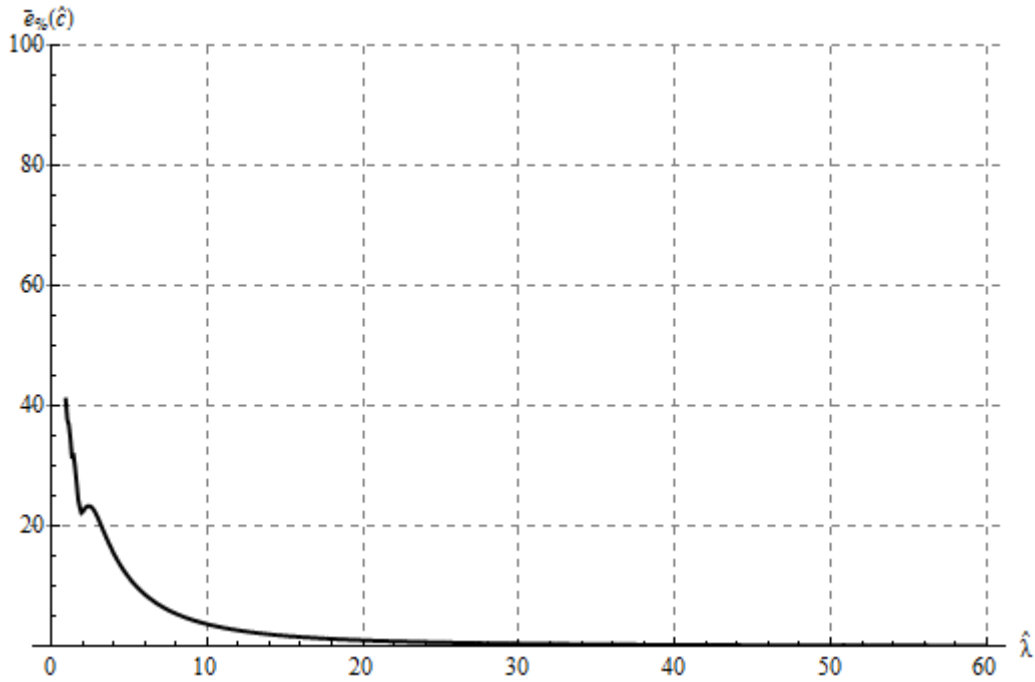


Figure 18. Average relative error between the discrete and the continuum description for the six oscillation modes for propagating waves in direction e_1 . The discrete and the continuum descriptions converge for large wavelengths.

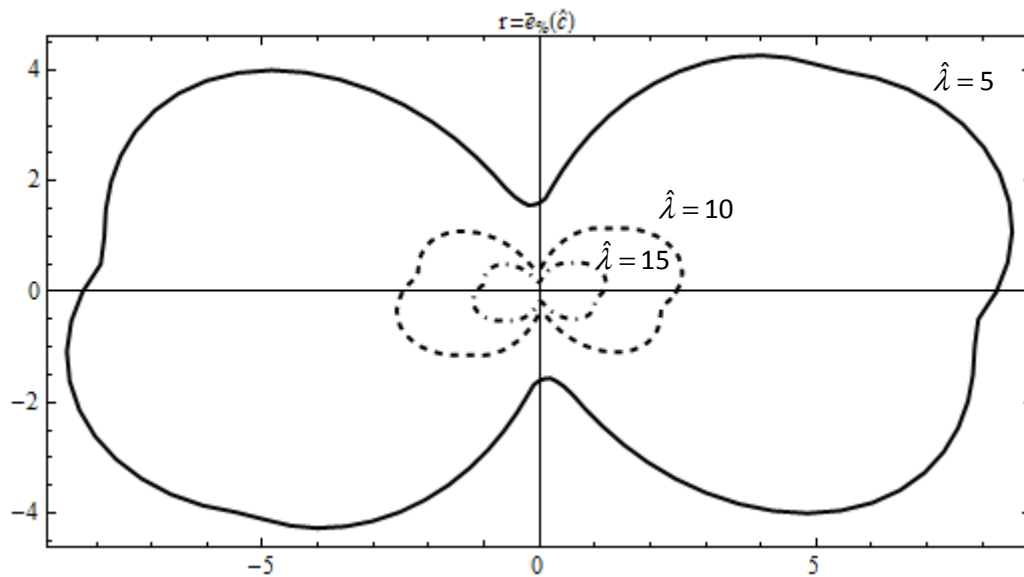


Figure 19. Polar plot of the average relative error of the discrete and the continuum description for propagating waves at all directions. The error is not uniform in all directions, because of the anisotropy of the structure.

The running-bond masonry pattern has been already studied in a previous paper and a Cosserat continuum was identified as an equivalent continuum for this discrete structure (Stefanou et al., 2008). Therefore, it is also interesting to compare these results with the present continuum in the limit case where $a_1 = \frac{a_2}{2}$ and $b_1 = 0$. In this case the running-bond

masonry pattern is geometrically retrieved (Figure 6). For deriving the discrete equations representing the running-bond from Eqs.(14) the stiffness coefficients of contacts Σ^2 , Σ^4 , Σ^6 and Σ^{10} have to be doubled. This is because the ‘big’ blocks interact through two springs with identical stiffness attached to the intermediate ‘small’ block of zero thickness (Figure 20).

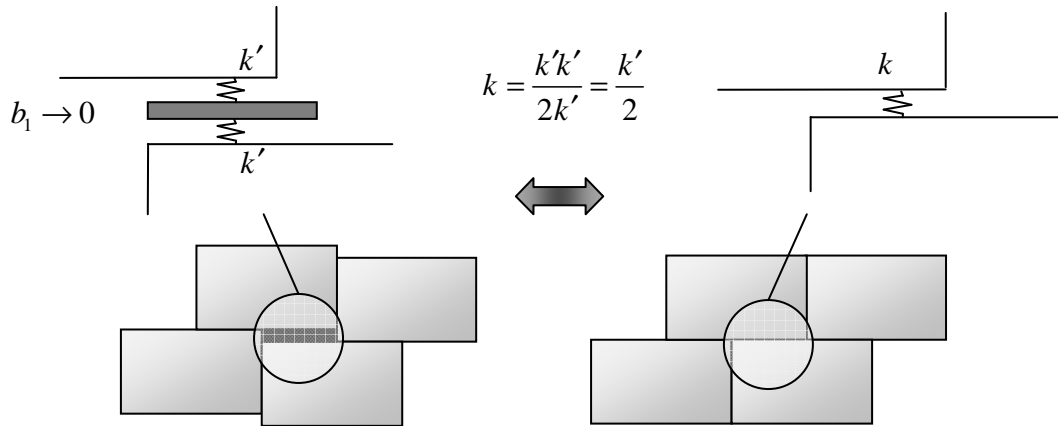


Figure 20. The limit case of the running-bond pattern: Replacement of the springs at contacts Σ^2 , Σ^4 , Σ^6 and Σ^{10} for deriving the discrete equations representing the running-bond masonry pattern.

For the aforementioned dimensions of the blocks $\mu_1 = 0$ and $\mu_2 = 1$. As mentioned in section 3, setting $\mu_1 = 0$ degenerates the micromorphic continuum considered here in a Cosserat continuum. Thus, a Cosserat type continuum is retrieved for the case of running-bond masonry. However, this does not imply that the two Cosserat continuum approximations are necessary identical, as the elementary cell, the kinematics and the constitutive law differ between them (cf. also (Salerno and de Felice, 2009)). This is demonstrated in terms of the dispersion functions. Figure 21 and figure 22 clearly show that the Cosserat continuum approximation obtained in Stefanou et al. (2008) is better for small wavelengths than the degenerated one from the present micromorphic approach. This better convergence can be explained by the geometry of the elementary cells and by noticing that the centers of neighboring elementary cells in the previous approach are closer to each other, (Figure 23), which reduces the residual of the Taylor expansion of the deformation measures (Eqs.(29)). One would expect the same convergence between the two approaches for $b_1 = b_2$, but this situation is not covered by the kinematics of the present micromorphic continuum as the condition $\Delta_2 \neq 0$ is violated (Eqs.(26)). If we wanted to allow the case $\Delta_2 = 0$, different kinematics should be derived from Eqs. (20) and (22). However, as explained above, the strategy was to eliminate the 3rd order terms $\chi_{ijk\ell}$ of the microdeformation measures and keep only terms of 2nd and lower order. In any case, the derived continua would be equivalent and only their convergence with the discrete model would have changed for small wavelengths.

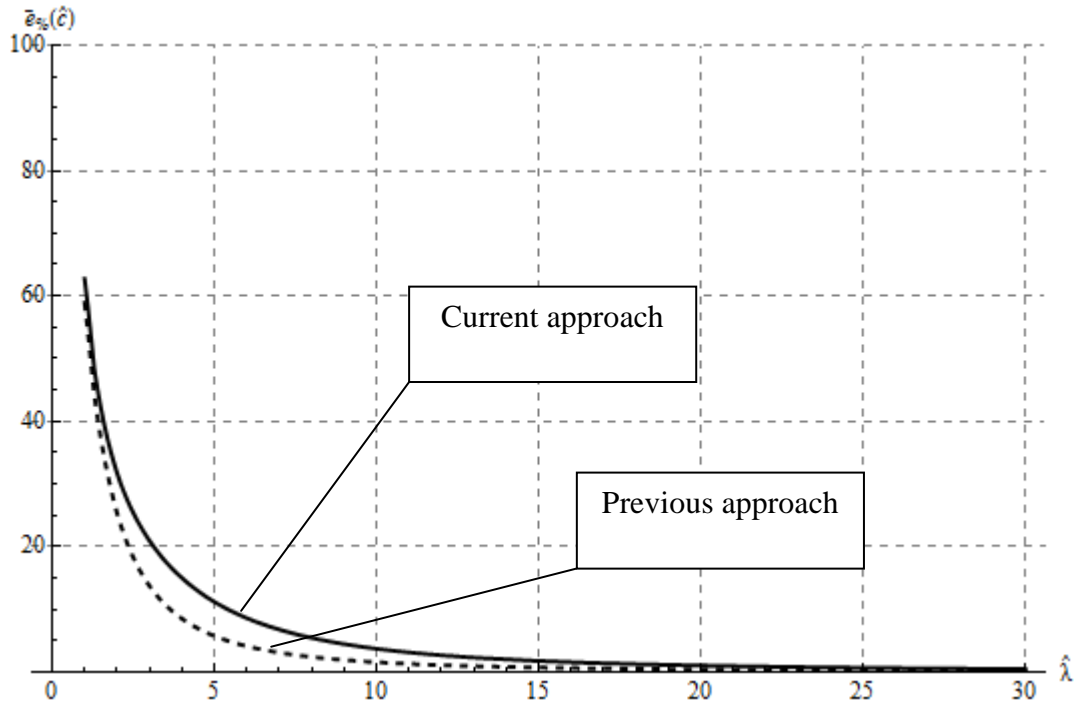


Figure 21. Average relative error between the discrete and the continuum description for the three oscillation modes for: a) the present approach with $a_1 = \frac{a_2}{2}$ and $b_1 = 0$ ($\mu_1 = 0$ - degenerated micromorphic resulting to Cosserat) and b) for the approach presented previously in Stefanou et al. (2008). Both continuum approximations converge for large wavelengths.

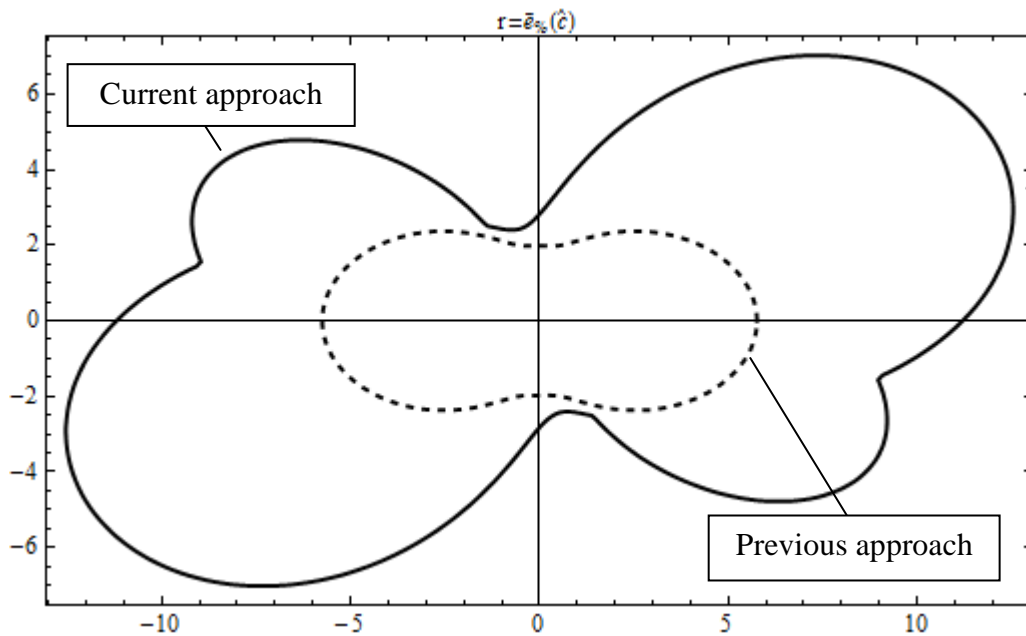


Figure 22. Polar plot of the average relative error between the discrete and the continuum description for propagating waves in all directions for: a) the present approach with $a_1 = \frac{a_2}{2}$ and $b_1 = 0$ ($\mu_1 = 0$ - degenerated micromorphic resulting to Cosserat) and b) for the

approach presented previously in Stefanou et al.(2008). The error is not uniform in all directions, because of the anisotropy of the structure.

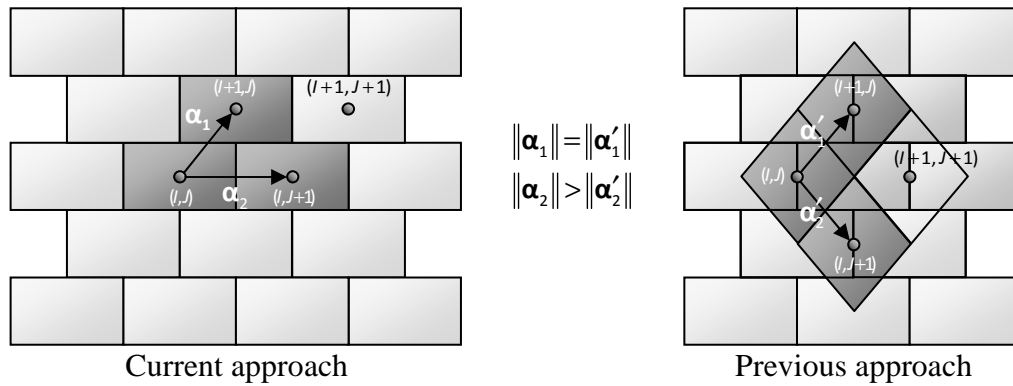


Figure 23. Repetition of elementary cells in space for: a) the present approach with $a_1 = \frac{a_2}{2}$ and $b_1 = 0$ ($\mu_1 = 0$ - degenerated micromorphic resulting to Cosserat continuum) and b) for the approach presented previously in Stefanou et al.(2008). The elementary cells are more distant in the present case leading to slower convergence of the dispersion functions of the continuum to the ones of the discrete structure.

5. Conclusions

In the classical paper of Germain in (1973) “The method of virtual power in Continuum Mechanics. Part 2: Micromechanics” the author writes:

“The theory [of the general micromorphic continuum...] is rich enough to fit various physical situations. The principal difficulty indeed is to discover the practical significance of some of the concepts which have been introduced, to design a method in order to exhibit their physical validity and to measure them in some specific physical situations.”

In the present paper an attempt was made to assess the significance of some of the quantities involved in the general theory of micromorphic media developed by Germain. This attempt was made by modeling an interlocking masonry wall as a discrete and as a continuum medium. The continuous description engaged a two dimensional, anisotropic, 2nd order micromorphic continuum, as lower order continua (e.g. classical Boltzmann, Cosserat, second gradient) cannot represent the complex kinematics of the aforementioned blocky structure. The method that was applied for the continuous approximation has its roots in the Differential Expansion homogenization technique (Pasternak and Mühlhaus, 2005) and differs from the Direct Averaging (Aboudi, 1991) and Asymptotic Averaging homogenization techniques (Bakhvalov and Panasenko, 1984; Sanchez-Palencia and Zaoui, 1987) in the sense that the latter are based on the averaging of the discrete quantities. In the present approach no averaging was made and consequently each dispersion curve of the discrete structure was approximated by the continuous model. Moreover, the approach

followed here avoids the ad-hoc omission of the higher order derivatives of the continuous fields for displacements and rotations that usually appear in other formulations (cf. also Bazant and Christensen, 1972; Eringen, 1999; Kumar and McDowell, 2004; Stefanou et al., 2008). Moreover, it avoids the identification by direct comparison of the terms of the PDE's of the continuum with the equations of the discrete system, after having replaced in the latter the discrete quotients by differential quotients based on Taylor expansions of some order (Eringen, 1999). Finally, the order of the Taylor expansion of the kinematic fields is not an a priori assumption of the method as it is in previous approaches. The necessary order of the Taylor expansion of the kinematic field of the continuum particle (Eq.(19)) is inferred by equating the degrees of freedom of the elementary cell of the discrete system with the equivalent measures of the particle itself (Eq.(20), (22)). Of course, the derived continuum is not unique and it depends on the initial choice of the elementary cell of the discrete structure. This is a rather well known issue (Novozhilov, 1961) and one should have in mind that the more blocks the elementary cell contains, the higher will be the order of the derived continuum.

Generally speaking, the philosophy of the present homogenization approach is rather inductive than deductive. The reason is that we start from the discrete system and we gradually build the equivalent continuum, while in other approaches the starting point is a general continuum of some order, which under various simplifications and assumptions is matched with the discrete system. The drawbacks of the latter approaches are that (a) the initially assumed higher order continuum may not describe adequately the kinematics of the discrete system, (b) the homogenized continuum might be difficult to handle because of the numerous parameters it embodies, (c) the physical meaning of the additional boundary conditions might be unclear and (d) in some extreme cases of identification, it may not satisfy basic conditions related to the positive definiteness of the elastic energy density (Mindlin, 1964).

The validity of the procedure followed herein was investigated by juxtaposing the dispersion functions of the discrete and the continuum models³. The results show that the continuum description is a large wavelength approximation of the discrete system. Nevertheless, the authors believe that the domain of validity of the continuous approximation can be extended to cover smaller wavelengths. This may be accomplished by enlarging the elementary cell to contain more blocks. The presence of more blocks in the elementary cell can cover high frequency oscillations between the blocks of the same cell, increasing, in this way, the accuracy of the continuum approximation in the dynamic regime when the wavelengths are small. The price for this better approximation is, of course, the additional complexity of the calculations as higher order continua are needed. However, in the majority of civil engineer

³ All the analytical calculations in the present paper have been performed with the symbolic language mathematical package Mathematica. The Mathematica files are available to the reader upon request to the corresponding author.

applications, large wavelength approximations are sufficient. In the present case the continuous model behaves well for wavelengths five times bigger than the characteristic length of the elementary cell. This means that the discrete and the continuous approximation share the same oscillation modes, have the same degrees of freedom, the same rigidity and the same inertia properties.

The present general interlocking masonry pattern can be degenerated to the running-bond masonry pattern, which was studied in detail by the authors in a previous paper. In this case, the micromorphic continuum derived here reduces to a Cosserat continuum describing the running-bond discrete masonry structure. The comparison of the dispersion curves of the current and the previous approach shows that both Cosserat approaches are equivalent to the discrete structure for wavelengths five times bigger the length of the building blocks. However, the elementary cell considered previously converges faster than the present one. This finding, demonstrates clearly that the elementary cell influences the accuracy of the derived continuum. The reason for this is attributed to the Taylor expansion of the macro- and micro-deformation measures.

Our analysis was limited in elasticity. However, the continuous model is general and can be expanded to cover non-linearities, as the expression of the various stress tensors in function of the internal forces and moments enable us to formulate yield surfaces and failure criteria based purely on micromechanical considerations. The flow rules are straightforward to derive as the kinematics of the continuum are directly matched to the kinematics of the discrete description. Therefore, the plastic and, more generally, the non-linear behavior of the interfaces of the blocks can be also considered and modeled accordingly. For practical structural applications a special Finite Element of 2nd order micromorphic continuum has to be programmed to account for the abovementioned non-linearities. However, the purpose of the present paper is to give the methodology of building a continuum that describes the presented general diatomic masonry wall pattern. The application to practical cases is the next step and will be presented in a future paper.

Acknowledgements

The authors would like to thank Professor H.G.Georgiadis (National Technical University of Athens) for the fruitful discussions and constructive comments. The research leading to these results has received funding from the European Research Council under the European Community's Seventh Framework Programme (FP7/2007-2013) / ERC grant agreement n° 228051.

References

- Aboudi, J., 1991. *Mechanics of composite materials. A unified micromechanical approach*. Amsterdam: Elsevier.
- Bakhvalov, N. and Panasenko, G., 1984. *Homogenisation: Averaging Process in Periodic Media*. Mathematics and Its Applications ed. Moscow: Nauca Publishers.

Bazant, Z.P. and Christensen, M., 1972. Analogy between micropolar continuum and grid frameworks under initial stress. *International Journal of Solids and Structures*, 8, pp.327-46.

Besdo, D., 1985. Inelastic behaviour of plane frictionless block-systems described as Cosserat media. *Arch. Mech. Meccanica*, 37, pp.603-19.

Bouras, M., Zambas, K. and Mavrommatis, S., 2002. The Works of the Committee for the Preservation of the Acropolis Monuments on the Acropolis of Athens. Athens: Hellenic Ministry.

Cecchi, A. and Sab, K., 2004. A comparison between a 3D discrete model and two homogenized plate models for periodic elastic brickwork. *International Journal of Solids and Structures*, 41, pp.2259-76.

Cecchi, A., Milani, G. and Tralli, A., 2007. A Reissner-Mindlin limit analysis model for out-of-plane loaded running bond masonry walls. *International Journal of Solids and Structures*, 44, pp.1438-60.

Cecchi, A. and Milani, G., 2008. A kinematic FE limit analysis model for thick English bond masonry walls. *International Journal of Solids and Structures*, 45, pp.1302-31.

Cerrolaza, M., Sulem, J. and Elbied, A., 1999. A Cosserat non-linear finite element analysis software for blocky structures. *Advanced Engineering Software*, 30, p.69-83.

Cosserat, E. and F., 1909. *Théorie de Corps déformables*. Paris.

Eringen, A.C., 1999. *Microcontinuum Field Theories I: Foundations and Solids*. New York: Springer-Verlag.

Ernst, B., 1983. *Der Zauberspiegel des M.C. Escher*. Deutscher Taschenbuch Verlag.

Georgiadis, H.G. and Velgaki, E.G., 2003. High-frequency Rayleigh waves in materials with microstructure and couple stress-effects. *International Journal of Solids and Structures*, 40, pp.2501-20.

Germain, P., 1973. The method of virtual power in continuum mechanics, Part 2: Microstructure. *SIAM Journal of Applied Mathematics*, 25, pp.556-75.

Kittel, C., 1996. *Introduction to Solid States Physics*. 7th ed. New York: John Wiley and Sons, Inc.

Kumar, R.S. and McDowell, D.L., 2004. Generalized continuum modelling of 2-D periodic cellular solids. *International Journal of Solids and Structures*, 41, pp.7399-422.

Masiani, R., Rizzi, N. and Trovalusci, P., 1995. Masonry walls as structured continua. *Meccanica*, 30, pp.673-83.

Milani, G., Lourenco, P.-B. and Tralli, A., 2006. Homogenised limit analysis of masonry walls, Part I: Failure surfaces. *Computers and Structures*, 84, pp.166-80.

Mindlin, R.D., 1964. Microstructure in linear elasticity. *Archive for Rational Mechanics and Analysis*, 16, pp.51-78.

Mindlin, R., 1965. Second gradient of strain and surface-tension in linear elasticity. *International Journal of Solids and Structures*, 1, pp.417-38.

Novozhilov, V.V., 1961. *Theory of Elasticity*. Pergamon Press.

Orduña, A. and Lourenço, P.B., 2005. Three-dimensional limit analysis of rigid blocks assemblages. Part I: Torsion failure on frictional interfaces and limit analysis formulation Generalised homogenization procedures for granular material. *International Journal of Solids and Structures*, 42, pp.5140-60.

Pasternak, E. and Mühlhaus, H.-B., 2005. Generalised homogenization procedures for granular material. *Journal of Engineering Mathematics*, 52, pp.199-229.

Raffard, D., 2000. *Modélisation de structures maçonnées par homogénéisation numérique non linéaire: application aux ouvrages d'intérêt archéologique*. France: PhD Thesis at Institut National Polytechnique de Lorraine.

Salerno, G. and de Felice, G., 2009. Continuum modeling of periodic brickwork. *International Journal of Solids and Structures*, 46, p.1251–1267.

Sanchez-Palencia, E. and Zaoui, A., 1987. *Homogenization techniques for composite media*. Berlin: Springer.

Stefanou, I., Sulem, J. and Vardoulakis, I., 2008. Homogenization of Interlocking Masonry Structures. In *3rd International W(H)YDOC*. Paris, 2008.

Stefanou, I., Sulem, J. and Vardoulakis, I., 2008. Three-dimensional Cosserat homogenization of masonry structures: elasticity. *Acta Geotechnica*, 3(1), pp.71-83.

Sulem, J. and Mühlhaus, H.-B., 1997. A continuum model for periodic two-dimensional block structures. *Mechanics of Cohesive-Frictional Materials*, 2, pp.31-46.

Vardoulakis, I. and Sulem, J., 1995. *Bifurcation analysis in geomechanics*. Glasgow: Blackie.

VITAE

(Authors' appearance in title order)



Ioannis Stefanou graduated in 2004 from the Civil Engineering School of National Technical University of Athens in Greece (NTUA). He has a master (a) in Structural Engineering and (b) in Applied Mechanics and a PhD in continuum modeling of discrete assemblies. During 2008-09, he was employed as a conservationist engineer in the Parthenon restoration site of Acropolis Hill in Athens. His main scientific interests are: (a) Dynamics of discrete-blocky systems with focus on classical monuments; (b) Discrete Element Modelling of blocky structures and (c) Homogenization of blocky periodic structures using Cosserat and higher order Continua. (<http://geolab.mechan.ntua.gr/people/stefanou/>)



Jean Sulem is Director of Research at Ecole Nationale des Ponts et Chaussées, which is one of the world's oldest engineering institutes. His research interests include bifurcation theory, constitutive modelling of continuous and discrete rock mass, experimental rock mechanics, coupled Thermo-Hydro-Mechanical behaviour of geomaterials with applications to civil and petroleum engineering, seismic risks, structural geology. He is the co-author of the book 'Bifurcation Analysis in Geomechanics' published with Prof. I. Vardoulakis in 1995. He has published 38 papers in International Journals and 61 communications in Conferences. (<http://navier.enpc.fr/~sulem/index.html>)



Ioannis Vardoulakis (1949-2009) was Professor of Mechanics in the Department of Applied Mathematics and Physics at National Technical University of Athens in Greece (NTUA). He obtained a Diploma of Civil Engineering (NTUA) and a PhD in soil Mechanics (University of Karlsruhe). He has been also a Professor of Geomechanics in the Department of Civil Engineering at the University of Minnesota in USA. He is an expert on mathematical modeling with major contributions in: (a) Constitutive modeling; (b) Computational mechanics; (c) Bifurcation and localization theory. He has more than 120 publications in refereed international journals and more than 90 announcements in conference proceedings. (<http://geolab.mechan.ntua.gr/people/vardoulakis/>)